

Spin-orbit-parity coupled superconductivity in topological monolayer WTe₂

Ying-Ming Xie,^{1,*} Benjamin T. Zhou,^{1,*} and K. T. Law^{1,†}

¹*Department of Physics, Hong Kong University of Science and Technology, Clear Water Bay, Hong Kong, China*

(Dated: January 15, 2022)

Recent experiments reported gate-induced superconductivity in the monolayer 1T'-WTe₂ which is a two-dimensional topological insulator in its normal state [1, 2]. The in-plane upper critical field B_{c2} is found to exceed the conventional Pauli paramagnetic limit B_p by 1-3 times. The enhancement cannot be explained by conventional spin-orbit coupling which vanishes due to inversion symmetry. In this work, we unveil some distinctive superconducting properties of centrosymmetric 1T'-WTe₂ which arise from the coupling of spin, momentum and band parity degrees of freedom. As a result of this spin-orbit-parity coupling (SOPC): (i) there is a first-order superconductor-metal transition at B_{c2} much higher than the Pauli paramagnetic limit B_p , (ii) spin-susceptibility is anisotropic with respect to in-plane directions and can result in possible anisotropic B_{c2} and (iii) the B_{c2} exhibits a strong gate dependence as the spin-orbit-parity coupling is significant only near the topological band crossing points. The importance of SOPC on the topologically nontrivial inter-orbital pairing phase is also discussed. Our theory generally applies to centrosymmetric materials with topological band inversions.

Introduction.— Recently, centrosymmetric monolayer 1T'-structure WTe₂, which is a two-dimensional topological insulator with helical edge states [3–7], has been found to become superconducting upon electro-gating [1, 2]. The coexistence of helical edge states and superconductivity establishes the system as a promising platform to create Majorana fermions [8, 9] and thus attracts wide on-going attention. Interestingly, the in-plane B_{c2} of the superconducting topological insulator was found to be 1-3 times higher than the usual Pauli paramagnetic limit B_p [1, 2].

It has been well established that spin-orbit couplings which lift spin degeneracies in electronic bands can enhance the B_{c2} in noncentrosymmetric superconductors [10, 11]. In particular, Ising superconductors such as non-centrosymmetric 2H-structure MoS₂, NbSe₂ and WS₂, have been shown to exhibit in-plane B_{c2} several times higher than B_p due to Ising spin-orbit coupling [12–23]. Despite similar chemical compositions and layered structures, 1T'-structure WTe₂ respects inversion symmetry such that spin-orbit coupling terms which involve only spin and momentum degrees of freedom are forbidden [3–5]. Therefore, the mechanism behind the observed enhancement of B_{c2} remains unknown.

In this work, we show that inversion symmetry allows the spin, momentum and parities of the electronic states to couple in 1T'-WTe₂. We refer to this coupling as spin-orbit-parity coupling (SOPC). The SOPC not only opens a topological gap (as depicted in Fig1), and creates the helical edge modes [3–7], but also pins the electron spins and renormalizes the effect of external Zeeman fields to enhance the B_{c2} . Importantly, the SOPC dramatically affects the superconducting properties such that: (i) 1T'-WTe₂ undergoes a first-order superconductor-metal transition at B_{c2} , similar to conventional s -wave superconductors [24]. However, the transition happens at a much higher field than B_p ; (ii) the spin susceptibil-

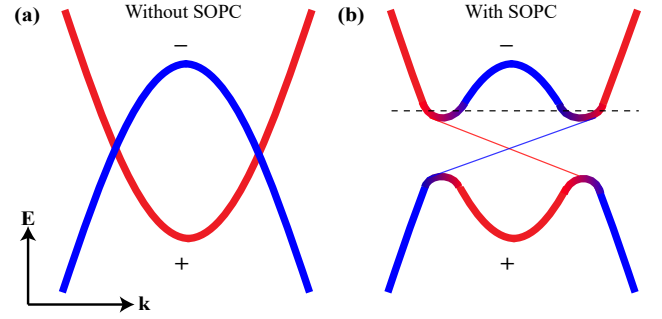


FIG. 1: Schematic band structure of two inverted bands without spin-orbit-parity coupling (SOPC) (a) and with SOPC coupling (b). The $+$ ($-$) sign labels the even (odd) parity of the band. Bands with even and odd parities in 1T'-WTe₂ originate predominantly from the d - and p - atomic orbitals respectively. In (b), the SOPC opens a topologically nontrivial gap at the band crossing points and edge states emerge (thin lines in the gap). Only states close to the crossing points with heavily mixed orbital parities can experience strong SOPC. The horizontal dashed line in (b) denotes the chemical potential at which superconductivity is observed in the experiment.

ity and B_{c2} can be anisotropic with respect to in-plane magnetic field directions; (iii) the B_{c2} is strongly gate-dependent as the SOPC is effective only for states near the topological band crossing points (band crossing involving bands with opposite parities). These properties distinguish superconductors with SOPC from noncentrosymmetric and conventional s -wave superconductors. Comparison among superconductors with SOPC, Ising superconductors and conventional s -wave superconductors is presented in Table I.

Importantly, SOPC widely exists in topological materials such as superconducting Cu-doped Bi₂Se₃ [25–28]. However, orbital depairing effects in three-dimensional materials overwhelm the Zeeman effect in the superconducting state. Moreover, superconductivity in Cu-doped

Bi_2Se_3 sets in when the chemical potential lies high above the band crossing points where the SOPC effect is weak [29, 30]. Therefore, atomically thin $1\text{T}'\text{-WTe}_2$, being superconducting near the band crossing points as depicted in Fig.1b, provides an ideal platform to study spin-orbit-parity coupled superconductivity. Interestingly, we further show that SOPC is important for stabilizing the inter-orbital pairing phases which can be topologically non-trivial.

Moreover, an enhanced B_{c2} has been observed in centrosymmetric monolayer $1\text{T}'\text{-MoTe}_2$ [31], which was attributed to Rashba spin-orbit coupling due to gate-induced inversion breaking. Our theory suggests that the B_{c2} enhancement in $1\text{T}'\text{-MoTe}_2$ can be readily explained by the SOPC and inversion breaking is inessential.

Model Hamiltonian of superconducting monolayer $1\text{T}'\text{-WTe}_2$.—The symmetry group of a monolayer $1\text{T}'\text{-WTe}_2$ is generated by time-reversal, one in-plane mirror symmetry, and spatial inversion. These symmetries dictate the form of a four-band $\mathbf{k}\cdot\mathbf{p}$ Hamiltonian which describes the normal state of WTe_2 [3, 32]:

$$H_0(\mathbf{k}) = \epsilon_0(\mathbf{k}) + \mathcal{M}(\mathbf{k})s_z + vk_xs_y + A_xk_xs_x\sigma_y + A_yk_ys_x\sigma_x + A_zk_ys_x\sigma_z, \quad (1)$$

where $\epsilon_0(\mathbf{k}) = t_x^+k_x^2 + t_y^+k_y^2 + \frac{1}{2}t'_xk_y^4 + \frac{1}{2}t'_yk_x^4 - \mu$, $\mathcal{M}(\mathbf{k}) = -\delta + t_x^-k_x^2 + t_y^-k_y^2 - \frac{1}{2}t'_xk_x^4 - \frac{1}{2}t'_yk_y^4$. Here, the s -matrices operate on the orbital degrees of freedom formed by (p , d)-orbitals with opposite parities, and σ -matrices act on the spin space. Notably, δ determines the order of the band at $\mathbf{k} = 0$. When $\delta > 0$, there is a band inversion while the SOPC terms open a topologically non-trivial gap and the system become a topological insulator as schematically depicted in Fig.1b. Derivation of the symmetry allowed terms and the model parameters are given in the Supplementary Materials [32]. In H_0 , the energy dispersions of the bands are given by $\xi_{\pm}(\mathbf{k})$ (as shown in Fig.2a), with each band being two-fold degenerate due to both the spatial inversion and time-reversal symmetries.

We emphasize that the usual spin-orbit coupling terms which involve \mathbf{k} and σ only are forbidden by inversion symmetry. However, it is possible to have an SOPC term $\hat{\mathbf{g}}\cdot\boldsymbol{\sigma}$, where $\hat{\mathbf{g}} = (A_yk_y, A_xk_x, A_zk_z)s_x$. Importantly, the SOPC term is proportional to s_x and $\langle\Psi(\mathbf{k})|\hat{\mathbf{g}}\cdot\boldsymbol{\sigma}|\Psi(\mathbf{k})\rangle$ is significant only for Ψ with strongly hybridized p - and d -orbitals. This happens only near the topological band crossing points as schematically depicted in Fig.1b. Interestingly, superconductivity in $1\text{T}'\text{-WTe}_2$ was observed experimentally when conduction band states near the band crossing points at $\pm Q$ are filled (Fig.2a) with charge density $n \sim 10^{13}\text{cm}^{-2}$ [1, 2]. Thus, $1\text{T}'\text{-WTe}_2$ is an ideal platform to study the effects of SOPC on superconductivity.

Assuming on-site attractive interactions to be dominant, the intra-orbital singlet-pairing phase is expected to be energetically favorable. In this case, the supercon-

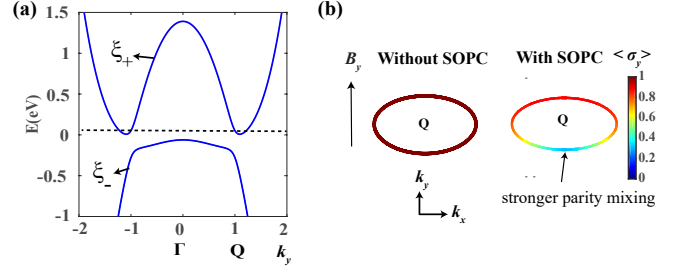


FIG. 2: (a) Normal-state band structure of monolayer WTe_2 . Hybridization between p - and d -bands from SOPC opens a topologically nontrivial gap near $\pm Q$ and results in two Q -valleys in the conduction bands. (b) Expectation value of spin- y component $\langle\sigma_y\rangle$ without(left)/with(right) SOPC on the Fermi surface contours under a weak Zeeman field $\mathbf{B} = B_y\hat{y}$ (Zeeman strength ~ 1 meV, contours around $+Q$ is shown here). The net spin along y -direction induced by B_y is reduced by the pinning due to SOPC.

ducting state under an in-plane magnetic field \mathbf{B} can be described by the Bogoliubovde Gennes Hamiltonian:

$$H_{BdG}(\mathbf{k}) = H_0(\mathbf{k})\eta_3 + \frac{1}{2}g_s u_B \mathbf{B} \cdot \boldsymbol{\sigma} + \Delta\eta_1, \quad (2)$$

where η operates on particle-hole space, u_B is the Bohr magneton, $g_s = 2$ is the Landé factor.

To understand how SOPC affects the magnetic response to an external Zeeman field, it is instructive to project $H_{BdG}(\mathbf{k})$ to a manifestly covariant pseudospin basis (MCPB) $\{|\mathbf{k}, \alpha\rangle, |\mathbf{k}, \beta\rangle\}$ [33–35] for the conduction band with energy $\xi_+(\mathbf{k})$, where superconducting pairing is formed. The transformation properties of the MCPB basis can be found in the Supplementary Materials [32]. By projecting $H_{BdG}(\mathbf{k})$ into the subspace $(\psi_{\mathbf{k},\alpha}^\dagger, \psi_{\mathbf{k},\beta}^\dagger, \psi_{-\mathbf{k},\beta}, -\psi_{-\mathbf{k},\alpha})$, the effective pairing Hamiltonian has the form:

$$H_{\text{eff}}(\mathbf{k}) = \xi_{\mathbf{k}}\eta_3 + \frac{1}{2}g_s u_B \mathbf{B} \cdot \tilde{\boldsymbol{\sigma}}(\mathbf{k}) + \Delta\eta_1, \quad (3)$$

where $\tilde{\sigma}_i^{l,l'}(\mathbf{k}) = \langle\mathbf{k}, l|\sigma_i|\mathbf{k}, l'\rangle = \sum_j a_{ij}(\mathbf{k})\rho_j^{l,l'}$ (ρ_j : Pauli matrix in the pseudospin basis) is the projected spin operator in the pseudospin subspace, and the effect of SOPC on electron spins are encoded in the coefficients $a_{ij}(\mathbf{k})$ (see Supplementary Material [32] for explicit forms of $a_{ij}(\mathbf{k})$). It is clear from Eq.3 that the Zeeman effect due to external magnetic fields is renormalized by the SOPC term.

To demonstrate the renormalization and the spin-pinning effect encoded in $a_{ij}(\mathbf{k})$, we assume a weak Zeeman field $\mathbf{B} = B_y\hat{y}$ in H_{eff} and plot the Zeeman field induced spin expectation value in the y -direction $\langle\sigma_y\rangle$ for states near the Q -point with and without SOPC in Fig.2b. Evidently, without SOPC, spins along the Fermi surface contours can freely align with B_y . In contrast, in the presence of SOPC, spins at different \mathbf{k} are pinned

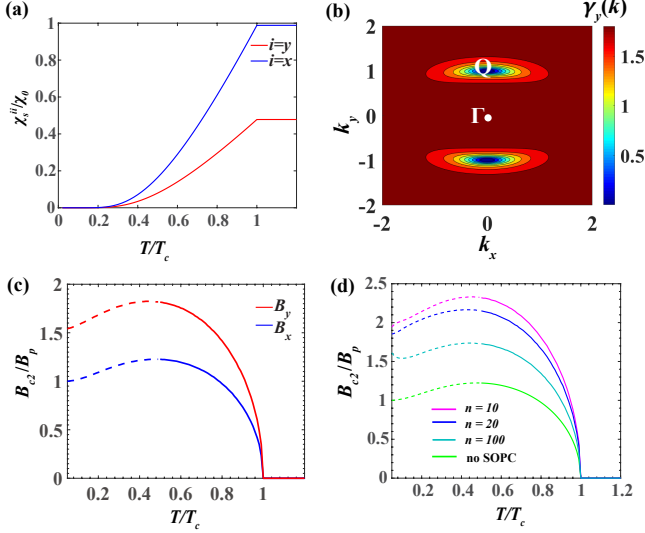


FIG. 3: Enhancement of B_{c2} via SOPC for 1T'-WTe₂. (a) Spin susceptibility χ_n^{ii} ($i = x, y$) as a function of temperature T , where the SOPC strength is $A_y = 0.855$ eV·Å, Fermi energy $E_F = 100$ meV. We set $T_c = 1$ K according to experimental observations. (b) Value of γ_y at different \mathbf{k} . $\gamma_y(\mathbf{k})$ approaches zero near the band minimum at $\pm Q$. (c) $B_{c2} - T_c$ curves for $\mathbf{B} = B_x \hat{x}$ (blue) and $\mathbf{B} = B_y \hat{y}$ (red). Other parameters are the same as in (a). (d) $B_{c2} - T_c$ curves for $\mathbf{B} = B_y \hat{y}$ with different carrier density n in units of 10^{12} cm⁻² and $A_y = 1.71$ eV·Å. The case without SOPC (light green curve) is presented for reference.

predominantly to the x -direction as the $A_y k_y s_x \sigma_x$ term dominates [32]. It is important to note that in Fig.2b, the spin pinning is much stronger for states with smaller k_y near the band crossing point due to the stronger mixing between p - and d -orbitals in these states. This clearly demonstrates the SOPC effect is not determined by the spin-orbit coupling part $A_y k_y \sigma_x$ alone, but also largely governed by the parity mixing operator s_x . In the next section, we show the important effects of SOPC on B_{c2} .

Enhancement, anisotropy and gate dependence of in-plane B_{c2} . —Phenomenologically, the normal-state and superconducting free energy densities due to an external in-plane field \mathbf{B} ($B = |\mathbf{B}|$) and pairing can be written as $f_n(B) = -\frac{1}{2}\chi_n B^2$, and $f_s(B) = f_{cond} + f_{spin}$ respectively. Here, χ_n/χ_s is the normal-state/superconducting spin susceptibility, $f_{cond} = -\frac{1}{2}N(E_F)\Delta_0^2$, with $\Delta_0 = \Delta(B = 0)$, is the zero-field condensation energy with $N(E_F)$ being the density of states at Fermi energy, and $f_{spin} = -\frac{1}{2}\chi_s B^2$ is the spin magnetic energy in the superconducting state. B_{c2} can be estimated by identifying the point $f_n(B) = f_s(B)$, yielding $B_{c2} \approx B_p \sqrt{\chi_0/(\chi_n - \chi_s)}$, where $B_p = \Delta_0/(\sqrt{2}\mu_B)$, and $\chi_0 = 2N(E_F)u_B^2$ is the Pauli spin susceptibility of free electron gas. Clearly, B_{c2} can be enhanced to be higher than B_p via: (i) a reduced $\chi_n < \chi_0$, and (ii) a residue $\chi_s \neq 0$. As shown in the MCPB basis, H_{eff} has the form of a spin-singlet super-

conductor, we expect that the superconducting ground state cannot respond to a weak external Zeeman fields, which implies $\chi_s = 0$ in the $T \rightarrow 0$ limit.

To demonstrate the vanishing χ_s in WTe₂, we calculate the superconducting spin susceptibility χ_s^{ii} ($i = x, y$) given by [36, 37]:

$$\begin{aligned} \chi_s^{ii} &= -\frac{1}{2}u_B^2 k_B T \sum_{\mathbf{k}, n} \text{Tr}[\tilde{\sigma}_i \mathcal{G}(\mathbf{k}, i\omega_n) \tilde{\sigma}_i \mathcal{G}(\mathbf{k}, i\omega_n)] \quad (4) \\ &= \frac{1}{2}u_B^2 \beta \sum_{\mathbf{k}} \gamma_i(\mathbf{k}) \frac{1}{1 + \cosh(\beta \sqrt{\xi_{\mathbf{k}}^2 + \Delta^2})}, \end{aligned}$$

where $\mathcal{G}(\mathbf{k}, i\omega_n) = (i\omega_n - \xi_{\mathbf{k}}\eta_3 - \Delta\eta_1)^{-1}$ is the Gor'kov Green's function obtained from $H_{eff}(\mathbf{k})$ in Eq.3 under zero magnetic field. T is the temperature, $\beta = 1/k_B T$, $\omega_n = (2n + 1)\pi/k_B T$ denotes the fermionic Matsubara frequency. $\gamma_i(\mathbf{k}) = 2 \sum_j a_{ij}^2(\mathbf{k})$ characterizes the renormalization effect on spins due to SOPC. Clearly, the denominator in the summand in Eq. (5) diverges as $T \rightarrow 0$ due to a finite superconducting gap Δ , thus $\chi_s^{ii}(T \rightarrow 0) = 0$ (Fig.3a).

The vanishing χ_s^{ii} leaves us with the mechanism of enhanced B_{c2} via reduced χ_n . Note that χ_n is directly given by $\chi_s(\Delta = 0)$ in Eq. (5), *i.e.*,

$$\chi_n^{ii} = \frac{1}{2}u_B^2 \beta \sum_{\mathbf{k}} \frac{\gamma_i(\mathbf{k})}{1 + \cosh(\beta \xi_{\mathbf{k}})} = u_B^2 N(E_F) \gamma_i(E_F), \quad (5)$$

where $\gamma_i(E_F) = \int d^2 \mathbf{k} \gamma_i(\mathbf{k}) \delta(\xi_{\mathbf{k}} - E_F) / \int d^2 \mathbf{k} \delta(\xi_{\mathbf{k}} - E_F)$ is the averaged renormalization factor due to SOPC over the Fermi surface (see Supplementary Material [32]).

As shown in Eq.5, the normal-state spin susceptibility is given by $\chi_n^{ii} = \gamma_i(E_F)\chi_0/2$, with a renormalization factor $\gamma_i(E_F)/2$ due to SOPC. In the low temperature limit, the in-plane critical field along i -direction ($i = x, y$) is directly related to the Pauli limit by $B_{c2}^i = B_p \sqrt{\chi_0/\chi_n^{ii}} = B_p \sqrt{2/\gamma_i(E_F)}$, which implies $B_{c2} > B_p$ when $\gamma_i(E_F) < 2$.

To show the reduced χ_n^{yy} , we plot $\gamma_y(\mathbf{k})$ in the conduction band (Fig.3b). Evidently, $\gamma_y(\mathbf{k}) < 2$ holds throughout the whole Brillouin zone. As a result, $\gamma_y(E_F) < 2$ in general, leading to $\chi_n^{yy} < \chi_0$ as consistent with the result in Fig.3a (red curve) where $\chi_s^{yy} = \chi_n^{yy} < \chi_0$ for $T > T_c$.

In contrast, we noticed that $\chi_s^{xx} = \chi_n^{xx} \approx \chi_0$ for $T > T_c$ (blue curve in Fig.3a). This is because $\mathbf{B} = B_x \hat{x}$ is collinear with the dominant SOPC term $A_y k_y s_x \sigma_x$ and thus can freely align spins to the x -direction. As a result, $B_{c2}^{yy} > B_p$ while $B_{c2}^{xx} \approx B_p$ as shown in the $B_{c2} - T_c$ curves in Fig.3c obtained by solving the linearized gap equation:

$$\frac{2}{U/V} = k_B T \sum_{\mathbf{k}, n} \text{Tr}[G^{(0)}(\mathbf{k}, i\omega_n) \rho_y G^{(0)T}(-\mathbf{k}, -i\omega_n) \rho_y]. \quad (6)$$

Here, U is electron-phonon interaction strength, V is the sample volume, $G^{(0)}(\mathbf{k}, i\omega_n)$ is the normal state Green's function of $H_{eff}(\mathbf{k})$ given in Eq. 3 (see Supplementary

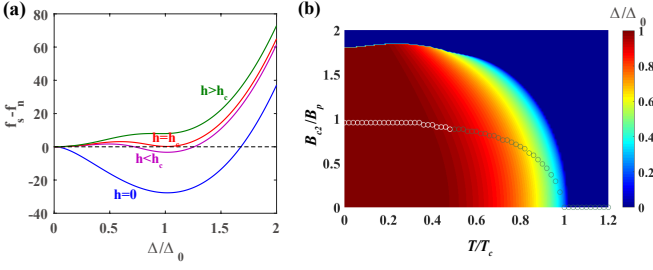


FIG. 4: (a) Landscapes of $f_s - f_n$ at $T = 0.1T_c$ in units of meV under $B = 0, 1.8B_p, 1.93B_p, 2.2B_p$. $B_{c2} \sim 1.93B_p$, with $\Delta_0 \approx 1.764k_B T_c$ at $B, T = 0$. (b) $B - T$ phase diagram from minimizing $f_s - f_n$ with $A_y = 1.71 \text{ eV}\cdot\text{\AA}$ and $n = 10 \times 10^{12} \text{ cm}^{-2}$. The color represents the magnitude of Δ at different B and T . The line of circles represent the values of B_{c2} in a conventional superconductor, where $B_{c2}(T = 0) = B_p$. A first-order transition also occurs in the low temperature regime [24] (indicated by white circles).

Materials [32] for details). Thus, our results suggest the B_{c2} of an SOPC superconductor can exhibit a strong anisotropy due to the anisotropic SOPC. This provides a distinctive signature of the possible SOPC origin behind the enhanced B_{c2} which is different from the isotropic B_{c2} and χ_s in both Ising superconductors and conventional superconductors as summarized in Table I.

Interestingly, $\gamma_y(\mathbf{k})$ has a strong \mathbf{k} -dependence (Fig.3b) with the renormalization being strongest (signified by a strongly reduced value of $\gamma_y(\mathbf{k})$) near the band crossing points at $\pm Q$. As E_F increases upon gating, outer Fermi circles enclosing $\pm Q$ are accessed and $\gamma_y(\mathbf{k})$ approaches $\gamma_0 = 2$ for free electron gas. This again reflects the *parity-mixing* nature of SOPC: the spin pinning effect due to SOPC terms is strongest near the band crossing points at $\pm Q$ where the p - and d -orbitals are strongly mixed. As \mathbf{k} deviates from $\pm Q$, the parity mixing becomes weaker and the spin pinning effect is suppressed. Such strong dependence of $\gamma_y(\mathbf{k})$ on Fermi level implies a strong gate-dependence in B_{c2}^{yy} . This is explicitly demonstrated by solving the linearized gap equation at different values of carrier density n (Fig.3d). Consistently, as n increases, the enhancement of B_{c2} is reduced.

Notably, for superconductors with SOPC, the low temperature sectors of the $B_{c2} - T_c$ curves obtained by linearized gap equations (dashed segments in the range $0 < T < T_1 \approx 0.5T_c$) do not represent the true values of B_{c2} but the supercooling critical field instead [24]. As we discuss next, the superconductor-metal transition at B_{c2} in this regime is in fact first-order in nature.

First-order phase transition at B_{c2} in low temperature regime.—To understand the nature of the phase transition at B_{c2} in the low temperature regime, we study how the free energy of a superconducting monolayer WTe₂ evolves under \mathbf{B} . Based on the full $H_{BdG}(\mathbf{k})$ in Eq.2, the free energy of the SOPC superconductor as a func-

tion of Δ can be obtained as [32, 38]:

$$f_s = \frac{V|\Delta|^2}{U} - \frac{1}{\beta} \sum_{\mathbf{k},n} \ln(1 + e^{-\beta\epsilon_{\mathbf{k},n}}), \quad (7)$$

where $\epsilon_{\mathbf{k},n}$ are the quasi-particle energies of $H_{BdG}(\mathbf{k})$. With fixed SOPC strength $A_y = 1.71 \text{ eV}\cdot\text{\AA}$ and carrier density $n = 10 \times 10^{12} \text{ cm}^{-2}$, the evolution of $f_s - f_n$ at $T = 0.1T_c$ under increasing B is shown in Fig.4a (note that $f_n \equiv f_s(\Delta = 0)$). Clearly, for $0 < B < B_{c2}$, a local minimum in the free energy landscape develops at $\Delta = 0$ (purple curve) and eventually becomes the global minimum at $B = B_{c2}$ (red curve), where the superconductor-metal transition occurs. Notably, Δ drops abruptly to zero at B_c , which signifies a first-order phase transition.

The full self-consistent $B - T$ phase diagram from minimizing $f_s - f_n$ is shown in Fig.4b with the phase boundary at B_{c2} accurately captured for all $T < T_c$. In accord with Fig.4a, the order parameter drops abruptly to zero at B_{c2} in the low temperature regime. We note that the mechanism of first-order transition in the low temperature limit for superconductors with SOPC is similar to a conventional superconductor, but the phase transition happens much higher than B_p in SOPC superconductors as illustrated in Fig.4b. In particular, this distinctive first-order transition in the SOPC superconductor WTe₂ is very different from the continuous phase transition found in noncentrosymmetric Ising superconductors such as NbSe₂ due to a significant χ_s induced by Ising spin-orbit couplings [18, 39, 40].

Conclusion and Discussions.— In this work, we identified a new class of centrosymmetric spin-orbit-parity coupled superconductors where SOPC leads to enhancement of in-plane B_{c2} higher than B_p . In particular, we explained how the strong parity-mixing due to SOPC near the topologically nontrivial gap edge gives rise to a strongly enhanced B_{c2} in the superconducting topological monolayer WTe₂ with low electron carrier density. We further pointed out that the B_{c2} of SOPC superconductors can exhibit an anisotropy in in-plane field directions (but the anisotropy has not yet been observed experimentally). These properties are distinguished from both conventional superconductors and Ising superconductors as summarized in Table I.

While we considered an SOPC superconductor in the clean limit, we briefly discuss here the effect of disorder. By including potential fluctuation scattering and spin-orbit scattering effects in the Green function and the vertex correction to χ_s , we show that the B_{c2} is not sensitive to potential fluctuation scattering but a finite χ_s is induced by spin-orbit scattering, which further enhances the B_{c2} [32]. This explains why a higher $B_{c2} \approx 4B_p$ was observed in the more disordered sample [1].

In the main text, we assumed intra-orbital pairing in Eq.2 belonging to the A_g representation of the C_{2h} point group. Here, we discuss the effect of an inter-

TABLE I: Comparison among centrosymmetric spin-orbit-parity-coupled(SOPC), Ising and conventional superconductivity.

Type of superconductors	SOPC	Ising	Conventional
Pairing correlations	Singlet	Singlet-triplet mixing	Singlet
$\chi_s(T=0)$	Zero	Finite	Zero
In-plane B_{c2}	$> B_p$	$> B_p$	$= B_p$
B -driven superconductor-metal transition as $T \rightarrow 0$	First-order	Continuous	First-order
Directional dependence of in-plane B_{c2}/χ_s	Anisotropic	Isotropic	Isotropic

orbital singlet pairing: $\hat{\Delta}_1 = \Delta_1 \eta_1 s_x$, which belongs to the B_u representation of C_{2h} . First, we show that the B_u phase can be favored only when the band mixing due to SOPC is strong because significant contributions from both parity-odd and parity-even orbitals at the Fermi energy are needed for the pairing to be effective [32]. Interestingly, such an odd-parity pairing leads to a DIII class topological superconductor when the Fermi surface encloses odd number of time-reversal-invariant-momentum(TRIM) points [27]. In fact, projecting $\hat{\Delta}_1$ to the MCPB basis explicitly reveals that the combination of $\hat{\Delta}_1$ and SOPC results in an effective $p_x \pm ip_y$ pairing [32].

Unfortunately, superconductivity in monolayer WTe₂ sets in when the Fermi surface consists of two disconnected Q -pockets away from the TRIM points (Fig.2). Thus, the system remains topologically trivial. Only by artificially tuning the chemical potential to enclose the Γ point, helical Majorana modes can emerge on the edge [32]. Moreover, the effective p -wave pairing can result in large χ_s^{yy} and divergent B_{c2}^{yy} which were not observed experimentally [1, 2]. Thus, we believe that the B_u phase is less likely to be manifested experimentally in WTe₂.

Note.—After presenting the main findings of this work [41], we noticed that the enhancement of B_{c2} was observed in non-topological centrosymmetric materials without band inversion such as in few-layer stanene and ultrathin PdTe₂ [42–44]. The enhanced B_{c2} in these materials originates mainly from k -independent atomic spin-orbital coupling, which is very different from the SOPC effect studied in this work.

Acknowledgments.—The authors thank Wenyu He, Noah F.Q. Yuan for discussions and Mengli Hu and Junwei Liu for showing us the band structure of 1T'-WTe₂ from first-principle calculations. KTL acknowledges the support of the Croucher Foundation and HKRGC through C6025-19G, C6026-16W, 16310219 and 16309718.

* These authors contributed equally to this work.

† Corresponding author.

phlaw@ust.hk

[1] V. Fatemi, S. Wu, Y. Cao, L. Bretheau, Q. D. Gibson,

- K. Watanabe, T. Taniguchi, R. J. Cava and P. Jarillo-Herrero, *Science* **362**, 926–929 (2018).
 [2] E. Sajadi, T. Palomaki, Z. Fei, W. Zhao, P. Bement, C. Olsen, S. Luescher, X. Xu, J. A. Folk and D. H. Cobden, *Science* **362**, 922–925 (2018).
 [3] X. Qian, J. Liu, L. Fu, and J. Li, *Science* **346**, 1344 (2014).
 [4] L. Muechler, A. Alexandradinata, T. Neupert, and R. Car, *Phys. Rev. X* **6**, 041069 (2016).
 [5] S. Tang et al., *Nat. Phys.* **13**, 683 (2017).
 [6] Z. Fei, T. Palomaki, S. Wu, W. Zhao, X. Cai, B. Sun, P. Nguyen, J. Finney, X. Xu and D. H. Cobden, *Nat. Phys.* **13**, 677 (2017).
 [7] S. Wu, V. Fatemi, Q. D. Gibson, K. Watanabe, T. Taniguchi, R. J. Cava, and P. Jarillo-Herrero, *Science* **359**, 76 (2018).
 [8] L. Fu and C. L. Kane, *Phys. Rev. B* **79**, 161408 (2009).
 [9] J. Nilsson, A. R. Akhmerov, and C. W. J. Beenakker, *Phys. Rev. Lett.* **101**, 120403 (2008).
 [10] P. A. Frigeri, D. F. Agterberg, A. Koga and M. Sigrist, *Phys. Rev. Lett.* **92**, 097001 (2004).
 [11] Gor'kov, Lev P. and Rashba, Emmanuel I., *Phys. Rev. Lett.* **87**, 037004 (2001).
 [12] Lu, J. M., Zheliuk, O., Leermakers, I., Yuan, N. F. Q., Zeitler, U., Law, K. T., Ye, J. T., *Science* **350**, 1353–1357 (2015).
 [13] X. Xi, Z. Wang, W. Zhao, J.-H. Park, K. T. Law, H. Berger, L. Forr, J. Shan, and K. F. Mak, *Nat. Phys.* **12**, 139 (2016).
 [14] Y. Saito et al., *Nature Physics* **12**, 144149 (2016).
 [15] S. C. de la Barrera, M. R. Sinko, D. P. Gopalan, N. Sivadas, K. L. Seyler, K. Watanabe, T. Taniguchi, A. W. Tsen, X. Xu, D. Xiao, and B. M. Hunt, *Nature Communications* **9**, 1427 (2018).
 [16] J. Lu, O. Zheliuk, Q. Chen, I. Leermakers, N. E. Hussey, U. Zeitler, and J. Ye, *Proc. Natl. Acad. Sci. U.S.A.* **115**, 3551 (2018).
 [17] Y. Xing, K. Zhao, P. Shan, F. Zheng, Y. Zhang, H. Fu, Y. Liu, M. Tian, C. Xi, H. Liu, J. Feng, X. Lin, S. Ji, X. Chen, Q.-K. Xue, and J. Wang, *Nano Lett.* **17**, 6802 (2017).
 [18] E. Sohn, X. Xi, W.-Y. He, S. Jiang, Z. Wang, K. Kang, J.-H. Park, H. Berger, L. Forró, K. T. Law, J. Shan, and K. F. Mak, *Nature Materials* **17**, 504 (2018).
 [19] B. T. Zhou, N. F. Q. Yuan, H.-L. Jiang, K. T. Law, *Phys. Rev. B* **93**, 180501 (2016).
 [20] W.-Y. He, B. T. Zhou, J. J. He, N. F. Q. Yuan, T. Zhang, K. T. Law, *Communications Physics* **1**, 40 (2018).
 [21] G. Sharma and S. Tewari, *Phys. Rev. B* **94**, 094515 (2016).
 [22] S. Ilić, J. S. Meyer, and M. Houzet, *Phys. Rev. Lett.* **119**, 117001 (2017).

- [23] J. Zhang and V. Aji, Phys. Rev. B **94**, 060501(R) (2016).
- [24] K. Maki and T. Tsuneto, Progress of Theoretical Physics **31**, 945 (1964).
- [25] H. Zhang, C.-X. Liu, X.-L. Qi, X. Dai, Z. Fang, and S.-C. Zhang, Nat. Phys. **5**, 438 (2009).
- [26] C.-X. Liu, X.-L. Qi, H. Zhang, X. Dai, Z. Fang, and S.-C. Zhang, Phys. Rev. B **82**, 045122 (2010).
- [27] L. Fu and E. Berg, Phys. Rev. Lett. **105**, 097001 (2010).
- [28] T. Hashimoto, K. Yada, A. Yamakage, M. Sato, and Y. Tanaka, Journal of the Physical Society of Japan **82**, 044704 (2013).
- [29] Y. S. Hor, A. J. Williams, J. G. Checkelsky, P. Roushan, J. Seo, Q. Xu, H. W. Zandbergen, A. Yazdani, N. P. Ong, and R. J. Cava, Phys. Rev. Lett. **104**, 057001 (2010).
- [30] L. A. Wray, S.-Y. Xu, Y. Xia, Y. S. Hor, D. Qian, A. V. Fedorov, H. Lin, A. Bansil, R. J. Cava, and M. Z. Hasan, Nat. Phys. **6**, 855 (2010).
- [31] D. Rhodes, N. F. Yuan, Y. Jung, A. Antony, H. Wang, B. Kim, Y.-c. Chiu, T. Taniguchi, K. Watanabe, K. Barmak, L. Balicas, C. R. Dean, X. Qian, L. Fu, A. N. Pasupathy, and J. Hone, arXiv:1905.06508 (2019).
- [32] See Supplemental Material for (1) $k \cdot p$ model of monolayer $1T'$ -WTe₂; (2) effective pairing Hamiltonian for SOPC superconductors; (3) Pauli spin susceptibility and renormalization factor γ_i ; (4) B_{c2} from the linearized gap equation; (5) derivation of superconducting free energy; (6) spin susceptibility with non-magnetic impurity scattering; (7) discussions on possible inter-orbital pairing phases.
- [33] S.-K. Yip, Phys. Rev. B **87**, 104505 (2013).
- [34] L. Fu, Phys. Rev. Lett. **115**, 026401 (2015).
- [35] J. W. F. Venderbos, V. Kozii, and L. Fu, Phys. Rev. B **94**, 180504 (2016).
- [36] P. A. Frigeri, D. F. Agterberg, and M. Sigrist, New Journal of Physics **6**, 115 (2004).
- [37] A. Abrikosov and L. Gorkov, Sov. Phys. JETP **15**, 752 (1962).
- [38] A. Altland and B. D. Simons, Condensed matter field theory (Cambridge University Press, 2010).
- [39] R. Wakatsuki and K. T. Law, arXiv:1604.04898 (2016).
- [40] Y. Xie, B. T. Zhou, T. K. Ng, and K. T. Law, Phys. Rev. Research **2**, 013026 (2020).
- [41] Y. Xie, W. He, and K. T. Law, in APS Meeting Abstracts (2019). <https://meetings.aps.org/Meeting/MAR19/Session/P09.5>.
- [42] C. Wang, B. Lian, X. Guo, J. Mao, Z. Zhang, D. Zhang, B.-L. Gu, Y. Xu, and W. Duan, Phys. Rev. Lett. **123**, 126402 (2019).
- [43] J. Falson, Y. Xu, M. Liao, Y. Zang, K. Zhu, C. Wang, Z. Zhang, H. Liu, W. Duan, K. He, H. Liu, J. H. Smet, D. Zhang, and Q.-K. Xue, Science **367**, 1454 (2020).
- [44] Y. Liu, Y. Xu, J. Sun, C. Liu, Y. Liu, C. Wang, Z. Zhang, K. Gu, Y. Tang, C. Ding, H. Liu, H. Yao, X. Lin, L. Wang, Q. Xue, and J. Wang, arXiv:1904.12719 (2019).

Supplementary Material for ‘Spin-orbit-parity coupled superconductivity in topological monolayer WTe₂’

Ying-Ming Xie,^{1,*} Benjamin T. Zhou,^{1,*} and K. T. Law^{1,†}

¹*Department of Physics, Hong Kong University of Science and Technology, Clear Water Bay, Hong Kong, China*
(Dated: January 15, 2022)

$\mathbf{k} \cdot \mathbf{p}$ MODEL OF MONOLAYER 1T'-WTe₂

Here, we present detailed derivation of the $\mathbf{k} \cdot \mathbf{p}$ Hamiltonian in Eq.1 of the main text based on the mirror symmetry M_y , inversion symmetry P and time reversal symmetry T . According to first principle calculations [S1–S6], the dominant orbitals near Γ point transforms as p_y and d_{yz} orbitals, which have opposite spatial parities and are odd under M_y . In the basis $(|p_y, \uparrow\rangle, |p_y, \downarrow\rangle, |d_{yz}, \uparrow\rangle, |d_{yz}, \downarrow\rangle)$, the symmetry operators are given by: $M_y = -i\sigma_y$, $P = s_z$, $T = i\sigma_y K$ [S7]. Using the method of invariant [S8], we write down a four-band $\mathbf{k} \cdot \mathbf{p}$ model as

$$H_0(\mathbf{k}) = \begin{pmatrix} \epsilon_p(\mathbf{k}) & 0 & -ivk_x + A_zk_y & -iA_xk_x + A_yk_y \\ 0 & \epsilon_p(\mathbf{p}) & iA_xk_x + A_yk_y & -ivk_x - A_zk_y \\ ivk_x + A_zk_y & -iA_xk_x + A_yk_y & \epsilon_d(\mathbf{k}) & 0 \\ iA_xk_x + A_yk_y & ivk_x - A_zk_y & 0 & \epsilon_d(\mathbf{k}) \end{pmatrix}, \quad (\text{S1})$$

where $\epsilon_p(\mathbf{k}) = -t_{xp}k_x^2 - t_{yp}k_y^2 - \mu_p$, $\epsilon_d(\mathbf{k}) = -t_{xd}k_x^2 - t_{yd}k_y^2 + t'_xk_x^4 + t'_yk_y^4 - \mu_d$. The effective parameters in Eq.S1 (listed in Table S1) are determined by fitting the *ab initio* band structure[S1, S2]. Note that $A_x, A_z < A_y$ due to the highly anisotropic crystal symmetry of 1T'-WTe₂ and the values of A_x, A_y, A_z in Table S1 are mainly as a reference for the scale, which is sensitive to the gap and hard to be solely determined by the *ab initio* calculation.

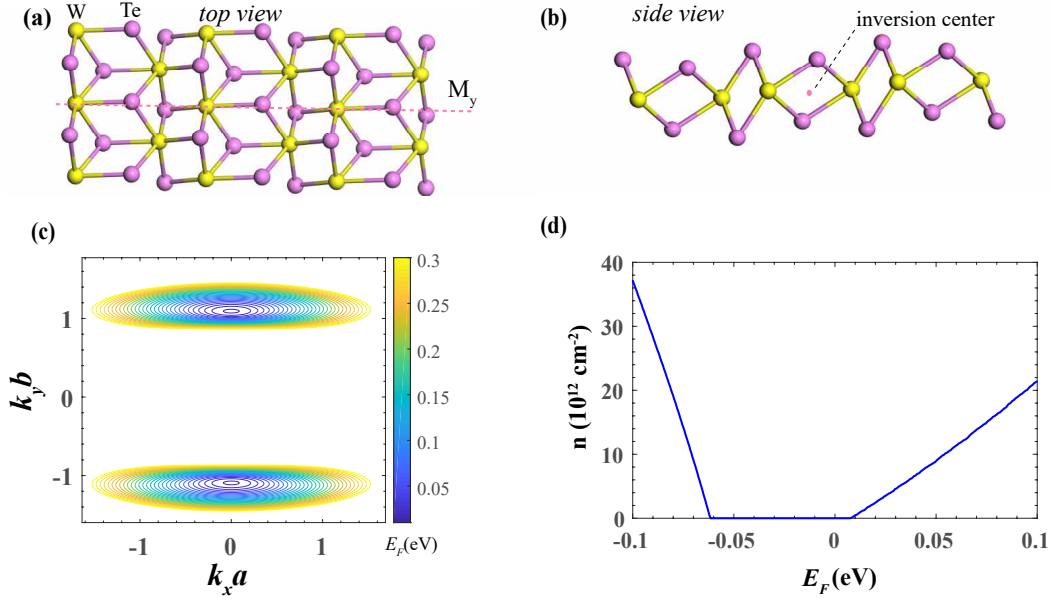


FIG. S1: Crystal structure and band structure of monolayer 1T'-WTe₂. (a) Top view and (b) side view of monolayer WTe₂. W/Te atoms are depicted in yellow/purple. M_y axis and inversion center are highlighted in pink dashed line and pink dot, respectively. (c) Fermi circles for Fermi energy E_F in the range $0 \sim 0.3$ eV from the model Hamiltonian (S1). The separation between adjacent Fermi circles is 0.01 eV. The corresponding parameters are listed in Table S1. (d) Carrier density $n = \langle \psi^\dagger(\mathbf{r})\psi(\mathbf{r}) \rangle$ versus E_F .

TABLE S1: Parameters of $\mathbf{k} \cdot \mathbf{p}$ Hamiltonian (S1). The lattice constants are $a = 6.31\text{\AA}$, $b = 3.49\text{\AA}$.

$\mu_p(\text{eV})$	$\mu_d(\text{eV})$	$t_{xp}(\text{eV} \cdot \text{\AA}^2)$	$t_{yp}(\text{eV} \cdot \text{\AA}^2)$	$t_{xd}(\text{eV} \cdot \text{\AA}^2)$	$t_{yd}(\text{eV} \cdot \text{\AA}^2)$	$t'_x(\text{eV} \cdot \text{\AA}^4)$	$t'_y(\text{eV} \cdot \text{\AA}^4)$	$v(\text{eV} \cdot \text{\AA})$	$A_x(\text{eV} \cdot \text{\AA})$	$A_y(\text{eV} \cdot \text{\AA})$	$A_z(\text{eV} \cdot \text{\AA})$
-1.39	0.062	12.45	18.48	-2.58	2.68	-7.79	26.65	2.34	0.17	0.57	0.07

EFFECTIVE PAIRING HAMILTONIAN FOR SOPC SUPERCONDUCTORS

The normal state electronic property is captured by the $\mathbf{k} \cdot \mathbf{p}$ model (Eq.S1). To further describe the superconducting topological monolayer WTe_2 , we first write down the Bogoliubovde Gennes Hamiltonian

$$H_{BdG}(\mathbf{k}) = H_0(\mathbf{k})\eta_3 + \frac{1}{2}gu_B\mathbf{B} \cdot \boldsymbol{\sigma} + \Delta\eta_1, \quad (\text{S2})$$

(same as Eq.2 of the main text). Here η_i is the Pauli matrix defined in the particle-hole basis. With the full $H_{BdG}(\mathbf{k})$, the spin susceptibility and free energy of the system can be readily calculated numerically. However, since superconducting pairing forms from states near Fermi energy only, we can further obtain an effective pairing Hamiltonian by projecting $H_0(\mathbf{k})$ to the conduction bands where the gate-induced superconductivity occurs. As mentioned in the main text, a convenient choice is the manifestly covariant pseudospin basis. In the following, we first derive the corresponding pseudospin basis $|\mathbf{k}, \alpha\rangle, |\mathbf{k}, \beta\rangle$ of the doubly degenerate conduction band. Then, we project the Hamiltonian $H_{BdG}(\mathbf{k})$ into the subspace $\{\psi_{\mathbf{k},\alpha}^\dagger, \psi_{\mathbf{k},\beta}^\dagger, \psi_{-\mathbf{k},\beta}, -\psi_{-\mathbf{k},\alpha}\}$, where $\psi_{\mathbf{k},\alpha}^\dagger, \psi_{\mathbf{k},\beta}^\dagger$ is the creation operator of $|\mathbf{k}, \alpha\rangle, |\mathbf{k}, \beta\rangle$.

Note that the Hamiltonian (S1) can be rewritten as

$$H_0(\mathbf{k}) = \epsilon_0(\mathbf{k}) + \mathcal{M}(\mathbf{k})s_z + vk_xs_y + A_xk_xs_x\sigma_y + A_yk_ys_x\sigma_x + A_zk_ys_x\sigma_z, \quad (\text{S3})$$

where

$$\epsilon_0(\mathbf{k}) = t_x^+k_x^2 + t_y^+k_y^2 + \frac{1}{2}t'_xk_y^4 + \frac{1}{2}t'_yk_y^4 - \mu_0, \quad (\text{S4})$$

$$\mathcal{M}(\mathbf{k}) = -\delta + t_x^-k_x^2 + t_y^-k_y^2 - \frac{1}{2}t'_xk_x^4 - \frac{1}{2}t'_yk_y^4. \quad (\text{S5})$$

Here $t_x^\pm = -(t_{xp} \pm t_{xd})/2$, $t_y^\pm = -(t_{yp} \pm t_{yd})/2$, $\mu_0 = (\mu_d + \mu_p)/2$, $\delta = (\mu_p - \mu_d)/2$. The spin-orbit-parity coupling(SOPC) terms are given by the $A_i(i = x, y, z)$ -terms involving the spin σ -matrices. Due to the presence of SOPC terms, we first diagonalize the spin part with the basis $|+1\rangle = \cos \frac{\theta_{\mathbf{k}}}{2} |\uparrow\rangle + \sin \frac{\theta_{\mathbf{k}}}{2} e^{i\phi_{\mathbf{k}}} |\downarrow\rangle$, $|-1\rangle = -\sin \frac{\theta_{\mathbf{k}}}{2} e^{-i\phi_{\mathbf{k}}} |\uparrow\rangle + \cos \frac{\theta_{\mathbf{k}}}{2} |\downarrow\rangle$. Here $\theta_{\mathbf{k}}$ and $\phi_{\mathbf{k}}$ are defined by $(A_yk_y, A_xk_x, A_zk_y) = Ak(\sin \theta_{\mathbf{k}} \cos \phi_{\mathbf{k}}, \sin \theta_{\mathbf{k}} \sin \phi_{\mathbf{k}}, \cos \theta_{\mathbf{k}})$. Then

$$H_0(\mathbf{k}) = \epsilon_0(\mathbf{k}) + \mathcal{M}(\mathbf{k})s_z + vk_xs_y + Ak_sx\tau_z. \quad (\text{S6})$$

τ_z is the Pauli matrix defined in $(|+1\rangle, |-1\rangle)$ space. By straightforward diagonalization, the eigenenergy can be obtained as $\epsilon_\pm(\mathbf{k}) = \epsilon_0(\mathbf{k}) \pm \sqrt{\mathcal{M}^2(\mathbf{k}) + v^2k_x^2 + A^2k^2}$, and each band has a two-fold degeneracy due to time-reversal and spatial inversion. The corresponding eigenvectors of the conduction band with $\epsilon_+(\mathbf{k})$ are given by

$$|\mathbf{k}, \alpha'\rangle = \frac{1}{N_{\mathbf{k}}} \begin{pmatrix} E(\mathbf{k}) + \mathcal{M}(\mathbf{k}) \\ ivk_x + Ak \end{pmatrix} \otimes \begin{pmatrix} \cos \frac{\theta_{\mathbf{k}}}{2} \\ \sin \frac{\theta_{\mathbf{k}}}{2} e^{i\phi_{\mathbf{k}}} \end{pmatrix}, \quad |\mathbf{k}, \beta'\rangle = \frac{1}{N_{\mathbf{k}}} \begin{pmatrix} E(\mathbf{k}) + \mathcal{M}(\mathbf{k}) \\ ivk_x - Ak \end{pmatrix} \otimes \begin{pmatrix} -\sin \frac{\theta_{\mathbf{k}}}{2} e^{-i\phi_{\mathbf{k}}} \\ \cos \frac{\theta_{\mathbf{k}}}{2} \end{pmatrix}, \quad (\text{S7})$$

where $E(\mathbf{k}) = \sqrt{\mathcal{M}^2(\mathbf{k}) + v^2k_x^2 + A^2k^2}$, the normalization factor $N_{\mathbf{k}} = \sqrt{(E(\mathbf{k}) + \mathcal{M}(\mathbf{k}))^2 + (v^2k_x^2 + A^2k^2)}$. We now construct the the pseudospin basis $|\mathbf{k}, \alpha\rangle, |\mathbf{k}, \beta\rangle$ with $|\mathbf{k}, \alpha'\rangle, |\mathbf{k}, \beta'\rangle$. Following the general scheme in Ref. [S9–S12], we first find the representation of spin operators, and construct a new basis formed by linear combinations of $|\mathbf{k}, \alpha'\rangle, |\mathbf{k}, \beta'\rangle$ under which the spin- z -component operator σ_z is diagonal. Then, we choose a proper phase factor such that the new basis vectors transform formally as spins under symmetry operations. Explicitly, the matrix representations

of spin in $(|\mathbf{k}, \alpha'\rangle, |\mathbf{k}, \beta'\rangle)^T$ are given by

$$\langle \sigma_x \rangle = \begin{pmatrix} \sin \theta_{\mathbf{k}} \cos \phi_{\mathbf{k}} & W_{\mathbf{k}} e^{-i\phi_{\mathbf{k}}} (\cos \theta_{\mathbf{k}} \cos \phi_{\mathbf{k}} + i \sin \phi_{\mathbf{k}}) \\ W_{\mathbf{k}}^* e^{i\phi_{\mathbf{k}}} (\cos \theta_{\mathbf{k}} \cos \phi_{\mathbf{k}} - i \sin \phi_{\mathbf{k}}) & -\sin \theta_{\mathbf{k}} \cos \phi_{\mathbf{k}} \end{pmatrix}, \quad (\text{S8})$$

$$\langle \sigma_y \rangle = \begin{pmatrix} \sin \theta_{\mathbf{k}} \sin \phi_{\mathbf{k}} & -i W_{\mathbf{k}} e^{-i\phi_{\mathbf{k}}} (\cos \phi_{\mathbf{k}} + i \cos \theta_{\mathbf{k}} \sin \phi_{\mathbf{k}}) \\ i W_{\mathbf{k}}^* e^{i\phi_{\mathbf{k}}} (\cos \phi_{\mathbf{k}} - i \cos \theta_{\mathbf{k}} \sin \phi_{\mathbf{k}}) & -\sin \theta_{\mathbf{k}} \sin \phi_{\mathbf{k}} \end{pmatrix}, \quad (\text{S9})$$

$$\langle \sigma_z \rangle = \begin{pmatrix} \cos \theta_{\mathbf{k}} & -W_{\mathbf{k}} e^{-i\phi_{\mathbf{k}}} \sin \theta_{\mathbf{k}} \\ -W_{\mathbf{k}}^* e^{i\phi_{\mathbf{k}}} \sin \theta_{\mathbf{k}} & -\cos \theta_{\mathbf{k}} \end{pmatrix}, \quad (\text{S10})$$

where $W_{\mathbf{k}} = \frac{(E(\mathbf{k}) + \mathcal{M}(\mathbf{k}))^2 - (A\mathbf{k} - i v k_x)^2}{N_{\mathbf{k}}^2}$. The positive eigenvalues of the above spin matrices are: $(\sqrt{\sin^2 \theta_{\mathbf{k}} \cos^2 \phi_{\mathbf{k}} + |W_{\mathbf{k}}|^2 (\cos^2 \theta_{\mathbf{k}} \cos^2 \phi_{\mathbf{k}} + \sin^2 \phi_{\mathbf{k}})}, \sqrt{\sin^2 \theta_{\mathbf{k}} \sin^2 \phi_{\mathbf{k}} + |W_{\mathbf{k}}|^2 (\cos^2 \theta_{\mathbf{k}} \sin^2 \phi_{\mathbf{k}} + \cos^2 \phi_{\mathbf{k}})}, \lambda_{\mathbf{k}})$, where $\lambda_{\mathbf{k}} = \sqrt{\cos^2 \theta_{\mathbf{k}} + |W_{\mathbf{k}}|^2 \sin^2 \theta_{\mathbf{k}}}$, $|W_{\mathbf{k}}|^2 = \sqrt{1 - A^2 k^2 / E^2(\mathbf{k})}$. By taking proper linear combinations of $|\mathbf{k}, \alpha'\rangle, |\mathbf{k}, \beta'\rangle$ [S9–S11], the pseudospin basis can be obtained as

$$|\mathbf{k}, \alpha\rangle = \frac{e^{-i\frac{\alpha_{\mathbf{k}}}{2}}}{\sqrt{|W_{\mathbf{k}}|^2 \sin^2 \theta_{\mathbf{k}} + (\cos \theta_{\mathbf{k}} - \lambda_{\mathbf{k}})^2}} (W_{\mathbf{k}} \sin \theta_{\mathbf{k}} |\mathbf{k}, \alpha'\rangle + (\cos \theta_{\mathbf{k}} - \lambda_{\mathbf{k}}) e^{i\phi_{\mathbf{k}}} |\mathbf{k}, \beta'\rangle) \quad (\text{S11})$$

$$|\mathbf{k}, \beta\rangle = \frac{e^{i\frac{\alpha_{\mathbf{k}}}{2}}}{\sqrt{|W_{\mathbf{k}}|^2 \sin^2 \theta_{\mathbf{k}} + (\cos \theta_{\mathbf{k}} - \lambda_{\mathbf{k}})^2}} ((\lambda_{\mathbf{k}} - \cos \theta_{\mathbf{k}}) e^{-i\phi_{\mathbf{k}}} |\mathbf{k}, \alpha'\rangle + W_{\mathbf{k}}^* \sin \theta_{\mathbf{k}} |\mathbf{k}, \beta'\rangle) \quad (\text{S12})$$

where $e^{i\alpha_{\mathbf{k}}} = \frac{W(\mathbf{k})}{|W(\mathbf{k})|}$. It is straightforward to see $T|\mathbf{k}, \alpha\rangle = |-\mathbf{k}, \beta\rangle$, $T|\mathbf{k}, \beta\rangle = -|-\mathbf{k}, \alpha\rangle$, $P|\mathbf{k}, \alpha\rangle = |-\mathbf{k}, \alpha\rangle$, $P|\mathbf{k}, \beta\rangle = |-\mathbf{k}, \beta\rangle$ (note that under time-reversal operation $\phi_{\mathbf{k}} \rightarrow \pi + \phi_{\mathbf{k}}$, $\theta_{\mathbf{k}} \rightarrow \pi - \theta_{\mathbf{k}}$, $\alpha_{\mathbf{k}} \rightarrow -\alpha_{\mathbf{k}}$). The representations of $\sigma_x, \sigma_y, \sigma_z$ in the pseudospin basis $\{|\mathbf{k}, \alpha\rangle, |\mathbf{k}, \beta\rangle\}$ are

$$\begin{aligned} \tilde{\sigma}_x(\mathbf{k}) &= \begin{pmatrix} \frac{1-|W_{\mathbf{k}}|^2}{2\lambda_{\mathbf{k}}} \sin(2\theta_{\mathbf{k}}) \cos \phi_{\mathbf{k}} & |W_{\mathbf{k}}| e^{-i\phi_{\mathbf{k}}} (\frac{\cos \phi_{\mathbf{k}}}{\lambda_{\mathbf{k}}} + i \sin \phi_{\mathbf{k}}) \\ |W_{\mathbf{k}}| e^{i\phi_{\mathbf{k}}} (\frac{\cos \phi_{\mathbf{k}}}{\lambda_{\mathbf{k}}} - i \sin \phi_{\mathbf{k}}) & \frac{|W_{\mathbf{k}}|^2 - 1}{2\lambda_{\mathbf{k}}} \sin(2\theta_{\mathbf{k}}) \cos \phi_{\mathbf{k}} \end{pmatrix} \\ &= |W_{\mathbf{k}}| (\frac{\cos^2 \phi_{\mathbf{k}}}{\lambda_{\mathbf{k}}} + \sin^2 \phi_{\mathbf{k}}) \rho_1 + |W_{\mathbf{k}}| \sin \phi_{\mathbf{k}} \cos \phi_{\mathbf{k}} (\frac{1}{\lambda_{\mathbf{k}}} - 1) \rho_2 + \frac{1 - |W_{\mathbf{k}}|^2}{2\lambda_{\mathbf{k}}} \sin(2\theta_{\mathbf{k}}) \cos \phi_{\mathbf{k}} \rho_3 \end{aligned} \quad (\text{S13})$$

$$\begin{aligned} \tilde{\sigma}_y(\mathbf{k}) &= \begin{pmatrix} \frac{1-|W_{\mathbf{k}}|^2}{2\lambda_{\mathbf{k}}} \sin(2\theta_{\mathbf{k}}) \sin \phi_{\mathbf{k}} & |W_{\mathbf{k}}| e^{-i\phi_{\mathbf{k}}} (\frac{\sin \phi_{\mathbf{k}}}{\lambda_{\mathbf{k}}} - i \cos \phi_{\mathbf{k}}) \\ |W_{\mathbf{k}}| e^{i\phi_{\mathbf{k}}} (\frac{\sin \phi_{\mathbf{k}}}{\lambda_{\mathbf{k}}} + i \cos \phi_{\mathbf{k}}) & \frac{|W_{\mathbf{k}}|^2 - 1}{2\lambda_{\mathbf{k}}} \sin(2\theta_{\mathbf{k}}) \sin \phi_{\mathbf{k}} \end{pmatrix} \\ &= |W_{\mathbf{k}}| \sin \phi_{\mathbf{k}} \cos \phi_{\mathbf{k}} (\frac{1}{\lambda_{\mathbf{k}}} - 1) \rho_1 + |W_{\mathbf{k}}| (\frac{\sin^2 \phi_{\mathbf{k}}}{\lambda_{\mathbf{k}}} + \cos^2 \phi_{\mathbf{k}}) \rho_2 + \frac{1 - |W_{\mathbf{k}}|^2}{2\lambda_{\mathbf{k}}} \sin(2\theta_{\mathbf{k}}) \sin \phi_{\mathbf{k}} \rho_3 \\ \tilde{\sigma}_z(\mathbf{k}) &= \lambda_{\mathbf{k}} \begin{pmatrix} 1 & 0 \\ 0 & -1 \end{pmatrix} = \lambda_{\mathbf{k}} \rho_3 \end{aligned} \quad (\text{S14})$$

For notational convenience, we define $\tilde{\sigma}_i(\mathbf{k}) = \sum_j a_{ij}(\mathbf{k}) \rho_j$. $a_{ij}(\mathbf{k})$ captures the effect of SOPC on the spin properties, ρ_j is the Pauli matrix defined in the pseudospin basis. It can be verified that under all symmetry operations, $\tilde{\sigma}_i(\mathbf{k})$ has the same transformation rules as spins. By projecting the full BdG Hamiltonian to the pseudospin basis, the pairing Hamiltonian is

$$H_s = \Delta \sum_{\mathbf{k}} c_{\mathbf{k}p,\uparrow}^\dagger c_{-\mathbf{k}p,\downarrow}^\dagger + c_{\mathbf{k}d,\uparrow}^\dagger c_{-\mathbf{k}d,\downarrow}^\dagger + h.c. \approx \Delta \sum_{\mathbf{k}} \psi_{\mathbf{k},\alpha}^\dagger \psi_{-\mathbf{k},\beta}^\dagger + h.c.. \quad (\text{S15})$$

Note that the form of s -wave pairing is preserved, *i.e.*, pseudospin-up and pseudospin-down states with opposite momentum are paired. This leads to the final form (as in Eq.3 of the main text) of the effective pairing Hamiltonian in the Nambu pseudospin basis $\Psi_{\mathbf{k}}^\dagger = (\psi_{\mathbf{k},\alpha}^\dagger, \psi_{\mathbf{k},\beta}^\dagger, \psi_{-\mathbf{k},\beta}, -\psi_{-\mathbf{k},\alpha})$:

$$H_{\text{eff}} = \sum_{\mathbf{k}, l, l'} \psi_{\mathbf{k}, l}^\dagger (\xi_+(\mathbf{k}) \delta_{l, l'} + \frac{1}{2} g_s u_B \mathbf{B} \cdot \tilde{\boldsymbol{\sigma}}_{l, l'}(\mathbf{k})) \psi_{\mathbf{k}, l'} + \Delta \sum_{\mathbf{k}} \psi_{\mathbf{k}, \alpha}^\dagger \psi_{-\mathbf{k}, \beta}^\dagger + h.c., \quad (\text{S16})$$

where l labels α, β , $\xi_{\pm}(\mathbf{k}) = \epsilon_0(\mathbf{k}) + E(\mathbf{k})$. In the following, we neglect the $+$ index, *i.e.*, $\xi_{\mathbf{k}} \equiv \xi_+(\mathbf{k})$.

PAULI SPIN SUSCEPTIBILITY AND RENORMALIZATION FACTOR γ_i

In general, the Pauli spin susceptibility with mean-field order parameter Δ is given by

$$\chi_s^{ij} = -\frac{1}{2}u_B^2 k_B T \sum_{\mathbf{k}} \sum_{\omega_n} \text{Tr}[\tilde{\sigma}_i \mathcal{G}^0(\mathbf{k}, i\omega_n) \tilde{\sigma}_j \mathcal{G}^0(\mathbf{k}, i\omega_n)]. \quad (\text{S17})$$

Here $\mathcal{G}^0(\mathbf{k}, i\omega_n) = (i\omega_n - \xi_{\mathbf{k}}\eta_3 - \Delta\eta_1)^{-1} = -\frac{i\omega_n + \xi_{\mathbf{k}}\eta_3 + \Delta\eta_1}{\omega_n^2 + \xi_{\mathbf{k}}^2 + \Delta^2}$ is the Nambu-Gor'kov Green's function. The factor 1/2 results from the particle-hole redundancy of Nambu basis. Eq.S17 is equivalent to the spin susceptibility formula given in Ref. [S13, S14]. By tracing out the pseudospin and particle-hole indices, we obtain

$$\chi_s^{ii} = -u_B^2 k_B T \sum_{\mathbf{k}} \sum_{\omega_n} \gamma_i(\mathbf{k}) \frac{-\omega_n^2 + \xi_{\mathbf{k}}^2 + \Delta^2}{(\omega_n^2 + \Delta^2 + \xi_{\mathbf{k}}^2)^2} \quad (\text{S18})$$

where $\gamma_i(\mathbf{k}) = 2 \sum_j a_{ij}^2(\mathbf{k})$ is the renormalization factor due to SOPCs, which are given explicitly by

$$\gamma_x(\mathbf{k}) = \frac{4|W_{\mathbf{k}}|^2 + (1 - |W_{\mathbf{k}}|^2)^2 \sin^2 2\theta_{\mathbf{k}}}{2(\cos^2 \theta_{\mathbf{k}} + |W_{\mathbf{k}}|^2 \sin^2 \theta_{\mathbf{k}})} \cos^2 \phi_{\mathbf{k}} + 2|W_{\mathbf{k}}|^2 \sin^2 \phi_{\mathbf{k}} \quad (\text{S19})$$

$$\gamma_y(\mathbf{k}) = \frac{4|W_{\mathbf{k}}|^2 + (1 - |W_{\mathbf{k}}|^2)^2 \sin^2 2\theta_{\mathbf{k}}}{2(\cos^2 \theta_{\mathbf{k}} + |W_{\mathbf{k}}|^2 \sin^2 \theta_{\mathbf{k}})} \sin^2 \phi_{\mathbf{k}} + 2|W_{\mathbf{k}}|^2 \cos^2 \phi_{\mathbf{k}} \quad (\text{S20})$$

$$\gamma_z(\mathbf{k}) = 2(\cos^2 \theta_{\mathbf{k}} + |W_{\mathbf{k}}|^2 \sin^2 \theta_{\mathbf{k}}). \quad (\text{S21})$$

By summing over the Matsubara frequencies in Eq.S18 first, the form of spin susceptibility can be further simplified to

$$\chi_s^{ii} = \frac{1}{2}u_B^2 \beta \sum_{\mathbf{k}} \gamma_i(\mathbf{k}) \frac{1}{1 + \cosh(\beta\sqrt{\xi_{\mathbf{k}}^2 + \Delta^2})}. \quad (\text{S22})$$

Note that at zero temperature, the residue spin susceptibility χ_s^{ii} vanishes since $\cosh(\beta\sqrt{\xi_{\mathbf{k}}^2 + \Delta^2}) \rightarrow \infty$. By taking $\Delta \rightarrow 0$, the normal-state spin susceptibility is recovered:

$$\chi_n^{ii} = \frac{1}{2}u_B^2 \beta \sum_{\mathbf{k}} \gamma_i(\mathbf{k}) \frac{1}{1 + \cosh(\beta\xi_{\mathbf{k}})} = u_B^2 N(E_F) \langle \gamma_i(E_F) \rangle. \quad (\text{S23})$$

Here $\langle \gamma_i(E_F) \rangle = \int d^2\mathbf{k} \gamma_i(\mathbf{k}) \delta(\xi_{\mathbf{k}} - E_F) / \int d^2\mathbf{k} \delta(\xi_{\mathbf{k}} - E_F)$ is the average value of γ_i over the Fermi surface. Obviously, in the zero temperature limit, the normal-state spin susceptibility is controlled by $\gamma_i(\mathbf{k})$, which can take a value within $[0, 2]$. To see how $\gamma_i(\mathbf{k})$ is affected by SOPCs, we note that if SOPC is absent, *i.e.*, $Ak = 0$, then $|W_{\mathbf{k}}| = 1$ and $\gamma_i = 2$. As we discussed in the main text, in this case the in-plane B_{c2} reduces to B_p . Upon increasing the SOPC strength, $|W_{\mathbf{k}}|$ is reduced, which reduces the value of $\gamma_i(\mathbf{k})$ and results in $B_{c2} > B_p$.

We note that there is another equivalent form of spin susceptibility obtained by performing the momentum integral first for Eq.S18:

$$\chi_s^{ii} / \chi_n^{ii} = 1 - \pi k_B T \sum_{\omega_n} \frac{\Delta^2}{(\Delta^2 + \omega_n^2)^{3/2}}, \quad (\text{S24})$$

where χ_n^{ii} is the reduced normal spin susceptibility. This form would provide a more straightforward way to understand disorder effects on the enhancement of B_{c2} as we shall discuss in details in Section VI.

B_{c2} FROM THE LINEARIZED GAP EQUATION

Here, we present details of the linearized gap equation we used to obtain the enhancement of B_{c2} shown in Fig.3 of the main text. Given the pairing Hamiltonian

$$H = \sum_{\mathbf{k}, l, l'} \psi_{\mathbf{k}, l}^\dagger (\xi_{\mathbf{k}} \delta_{l, l'} + u_B \mathbf{B} \cdot \tilde{\boldsymbol{\sigma}}) \psi_{\mathbf{k}, l'} - \frac{U}{2V} \sum_{\mathbf{k}, \mathbf{k}'} \psi_{\mathbf{k}, \alpha}^\dagger \psi_{-\mathbf{k}, \beta}^\dagger \psi_{-\mathbf{k}', \beta} \psi_{\mathbf{k}', \alpha}, \quad (\text{S25})$$

the corresponding linearized gap equation is given by

$$\frac{2}{U/V} = k_B T \sum_{\mathbf{k}} \sum_n \text{Tr}[G^{(0)}(\mathbf{k}, i\omega_n) \rho_y G^{(0)T}(-\mathbf{k}, -i\omega_n) \rho_y]. \quad (\text{S26})$$

Upon further simplifications and Matsubara sum, we have

$$\frac{1}{U/V} = k_B T \sum_{\mathbf{k}} \sum_n \frac{(i\omega_n - \xi_{\mathbf{k}})(-i\omega_n - \xi_{\mathbf{k}}) - u_B^2 \sum_j (\sum_i a_{ij}(\mathbf{k}) B_i)^2}{((i\omega_n - \xi_{\mathbf{k}})^2 - u_B^2 \sum_j (\sum_i a_{ij}(\mathbf{k}) B_i)^2)((-i\omega_n - \xi_{\mathbf{k}})^2 - u_B^2 \sum_j (\sum_i a_{ij}(\mathbf{k}) B_i)^2)}, \quad (\text{S27})$$

$$\frac{1}{U/V} = k_B T \sum_{\mathbf{k}} \frac{\sinh \beta \xi}{2\xi (\cosh \beta \xi + \cosh(\beta u_B B_{eff}(\mathbf{k})))}, \quad (\text{S28})$$

where $B_{eff} = \sqrt{\sum_i (a_{ij}(\mathbf{k}) B_i)^2}$. For magnetic field along the i -direction, $B_{eff} = B_i \sqrt{\gamma_k/2}$. In the absence of magnetic fields,

$$\frac{1}{U/V} = k_B T_c \sum_{\mathbf{k}} \frac{\sinh \beta \xi}{2\xi (\cosh \beta \xi + 1)} = k_B T_c N(E_F) \int_{-\hbar\omega_D}^{\hbar\omega_D} d\xi \frac{\tanh \beta \xi / 2}{2\xi} = N(E_F) \ln\left(\frac{2e^\gamma \hbar\omega_D}{\pi k_B T_c}\right), \quad (\text{S29})$$

Here, γ is the Euler constant, T_c is the zero field critical temperature. Substituting the expression of $\frac{1}{U/V}$ in Eq.S29 into Eq.S27, we get

$$\ln\left(\frac{T}{T_c}\right) = \int_{-\infty}^{+\infty} d\xi \int_0^{2\pi} \frac{d\varphi}{2\pi} \frac{\sinh \beta \xi}{2\xi} \left(\frac{1}{\cosh \beta \xi + \cosh(\beta u_B B_{eff}(E_F, \varphi))} - \frac{1}{\cosh \beta \xi + 1} \right) \quad (\text{S30})$$

Due to the complicated $a_{ij}(\mathbf{k})$ coefficients, the linearized gap equation was solved numerically by transforming the energy integral into a summation over momentum.

DERIVATION OF SUPERCONDUCTING FREE ENERGY

As we discussed in the main text, the scheme of linearized gap equation fails to capture the first-order phase transition at B_{c2} for the centrosymmetric spin-orbit-parity coupled(SOPC) superconductor WTe₂. As the in-plane field increases and approaches the superconductor-metal phase boundary, the superconducting gap and the value of B_{c2} need to be determined self-consistently by the minimum of the superconducting free energy f_s of the system. Here, we present a detailed derivation of the expression of f_s in the main text, which allows us to obtain the evolution of f_s under magnetic fields and the full superconducting phase diagram shown in Fig.4 of the main text.

In general, the partition function of a system involving two-body interactions can be written as:

$$Z = \int D[\psi(\mathbf{r}, \tau), \bar{\psi}(\mathbf{r}, \tau)] \exp\{-S[\psi(\mathbf{r}, \tau), \bar{\psi}(\mathbf{r}, \tau)]\}, \quad (\text{S31})$$

where the action is given by

$$S[\psi, \bar{\psi}] = \int d\tau \int d\mathbf{r} \sum_{\sigma} \bar{\psi}(\mathbf{r}, \tau) \partial_{\tau} \psi(\mathbf{r}, \tau) + \sum_{\sigma\sigma'} \bar{\psi}_{\sigma}(\mathbf{r}, \tau) H_0(\mathbf{r}, \tau) \psi_{\sigma'}(\mathbf{r}, \tau) - g \sum_{\sigma\sigma'} \bar{\psi}_{\sigma}(\mathbf{r}, \tau) \bar{\psi}_{\sigma'}(\mathbf{r}, \tau) \psi_{\sigma'}(\mathbf{r}, \tau) \psi_{\sigma}(\mathbf{r}, \tau). \quad (\text{S32})$$

By introducing an auxiliary bosonic field, the interaction term can be reformulated via the Hubbard-Stratonovich transformation:

$$\exp(g \int d\tau \int d\mathbf{r} \bar{\psi}_{\uparrow} \bar{\psi}_{\downarrow} \psi_{\downarrow} \psi_{\uparrow}) = \int D[\bar{\Delta}, \Delta] \exp(- \int d\tau \int d\mathbf{r} [\frac{1}{g} |\Delta|^2 - \Delta \bar{\psi}_{\uparrow} \bar{\psi}_{\downarrow} - \bar{\Delta} \psi_{\downarrow} \psi_{\uparrow}]), \quad (\text{S33})$$

Then, the action becomes

$$Z = \int D[\bar{\psi}(\mathbf{r}, \tau), \psi(\mathbf{r}, \tau)] \int D[\bar{\Delta}, \Delta] \exp(-S). \quad (\text{S34})$$

Here

$$S = \frac{1}{2} \int d\tau \int d\mathbf{r} \bar{\Phi} G^{-1} \Phi + \frac{1}{g} |\Delta|^2, \quad (\text{S35})$$

where $\Phi = (\bar{\psi}_\uparrow, \bar{\psi}_\downarrow, \psi_\uparrow, \psi_\downarrow)$ and

$$G^{-1} = \begin{pmatrix} \partial_\tau + H_0 & \Delta i\sigma_y \\ (\Delta i\sigma_y)^\dagger & \partial_\tau - H_0^* \end{pmatrix}. \quad (\text{S36})$$

Integrate out the Grassman field $\psi(\mathbf{r}, \tau)$, we have

$$Z = \int D[\bar{\Delta}, \Delta] \exp(-S_{eff}), \quad (\text{S37})$$

where $S_{eff} = \int d\tau \int d\mathbf{r} \frac{1}{g} |\Delta|^2 + \ln \text{Det} G^{-1}$. Within the mean-field approximation, Δ is assumed to be uniform in space and time. This reduces the mean-field free energy to the form

$$f_s = \frac{1}{\beta} \ln(Z) = \frac{1}{\beta} S_{eff} = \frac{V}{g} |\Delta|^2 - \frac{1}{\beta} \ln \text{Det} G^{-1} = \frac{V}{g} |\Delta|^2 - \frac{1}{\beta} \sum_{\mathbf{k}, n} \ln(1 + e^{-\beta \epsilon_{\mathbf{k}, n}}). \quad (\text{S38})$$

Here, V is the volume of system. The quasi-particle energies $\epsilon_{\mathbf{k}, n}$ are calculated from the full Bogoliubovde Gennes Hamiltonian $H_{BdG} = H_0(\mathbf{k})\eta_3 + \frac{1}{2}g_s u_B \mathbf{B} \cdot \boldsymbol{\sigma} + \Delta\eta_1$.

SPIN SUSCEPTIBILITY WITH NON-MAGNETIC IMPURITY SCATTERING

We discussed briefly in the main text that the enhancement of B_{c2} in SOPC superconductor is not affected in a qualitative way by disorder. Here we present detailed analysis of disorder effects on the SOPC superconductor WTe₂. Including both local potential fluctuation and spin-orbit scattering, the non-magnetic impurity potential can be written as [S15]

$$U_{im}(\mathbf{k} - \mathbf{k}') = U_1(\mathbf{k} - \mathbf{k}')\eta_3 + U_2(\mathbf{k} - \mathbf{k}')i(\hat{\mathbf{k}} \times \hat{\mathbf{k}}') \cdot \boldsymbol{\sigma}\eta_3 \quad (\text{S39})$$

$$= U_1(\mathbf{k} - \mathbf{k}')\eta_3 + U_2(\mathbf{k} - \mathbf{k}')i\lambda_{\mathbf{k}}\rho_3\eta_3(\hat{\mathbf{k}} \times \hat{\mathbf{k}}') \cdot \hat{z} \quad (\text{S40})$$

The diagrammatic calculation process to obtain the disorder-averaged spin susceptibility under $U_{im}(\mathbf{k} - \mathbf{k}')$ is shown in Fig.S2: following similar procedures in previous works [S14–S18], we first calculate the self-energy correction with the standard Born approximation. Then, we calculate the ladder diagram for the spin vertex correction, and finally obtain the disorder-averaged spin susceptibility as:

$$\overline{\chi_s^{ij}} = -\frac{1}{2}u_B^2 k_B T \sum_{\mathbf{k}} \sum_{\omega_n} \text{Tr}[\tilde{\sigma}_i \mathcal{G}(\mathbf{k}, i\omega_n) \Pi(\mathbf{k}, i\omega_n) \cdot \tilde{\sigma}_j \mathcal{G}(\mathbf{k}, i\omega_n)]. \quad (\text{S41})$$

Here $\mathcal{G}(\mathbf{k}, i\omega_n) = (i\omega_n - \xi_{\mathbf{k}}\eta_3 - \Delta\eta_1 - \Sigma(\mathbf{k}, i\omega_n))^{-1}$ is the Nam-Gor'kov Green's function including the self-energy correction due to disorder. The self-energy $\Sigma(\mathbf{k}, i\omega_n)$ is given by the self-consistent equation

$$\Sigma(\mathbf{k}, i\omega_n) = \int_{\mathbf{k}'} U_{im}(\mathbf{k} - \mathbf{k}') \mathcal{G}(\mathbf{k}', i\omega_n) U_{im}(\mathbf{k}' - \mathbf{k}), \quad (\text{S42})$$

where $\int_{\mathbf{k}} \equiv \int \frac{d^2\mathbf{k}}{(2\pi)^2}$. Within the Born approximation, the equation can be solved as

$$\Sigma(\mathbf{k}, i\omega_n) = -\frac{i\omega_n}{\tau\sqrt{\omega_n^2 + \Delta^2}} + \frac{\Delta}{\tau\sqrt{\omega_n^2 + \Delta^2}}\eta_1, \quad (\text{S43})$$

where $1/\tau = 1/\tau_0 + 1/\tau_{so}$ with

$$\frac{1}{\tau_0} = \pi N(E_F) \int d^2\mathbf{k}' \delta(\xi_{\mathbf{k}'} - E_F) |U_1(\mathbf{k} - \mathbf{k}')|^2, \quad (\text{S44})$$

$$\frac{1}{\tau_{so}} = \pi N(E_F) \int d^2\mathbf{k}' \delta(\xi_{\mathbf{k}'} - E_F) \lambda_{\mathbf{k}}^2 |U_2(\mathbf{k} - \mathbf{k}')|^2 \sin^2 \varphi_{\mathbf{k}'}. \quad (\text{S45})$$

Here, τ is the total scattering time, τ_0 is the momentum relaxation time, τ_{so} is the spin-orbit scattering time. Similar to previous works [S14, S16–S18], we consider the leading order s -wave scattering channel only, thus τ can be treated as \mathbf{k} -independent. Then $\mathcal{G}(\mathbf{k}, i\omega_n)$ can be rewritten as $\mathcal{G}(\mathbf{k}, i\omega_n) = (i\tilde{\omega}_n - \xi_{\mathbf{k}}\eta_3 - \tilde{\Delta}\eta_1)^{-1}$, where

$$\tilde{\omega}_n = \omega_n + \frac{\omega_n}{\tau\sqrt{\omega_n^2 + \Delta^2}}, \quad \tilde{\Delta} = \Delta + \frac{\Delta}{\tau\sqrt{\omega_n^2 + \Delta^2}}. \quad (\text{S46})$$

Now, we use $\mathcal{G}(\mathbf{k}, i\omega)$ to calculate the spin vertex corrections. The recursive integral equation for vertex correction, as depicted by the Feynman diagram Fig.S2d, is given by

$$\Pi(\mathbf{k}, i\omega_n) \cdot \tilde{\sigma}_j = \tilde{\sigma}_j + \int_{\mathbf{k}'} U_{im}(\mathbf{k} - \mathbf{k}') \mathcal{G}(\mathbf{k}', i\omega_n) \Pi(\mathbf{k}', i\omega_n) \cdot \tilde{\sigma}_j \mathcal{G}(\mathbf{k}', i\omega_n) U_{im}(\mathbf{k}' - \mathbf{k}) \quad (\text{S47})$$

Here, $\Pi(\mathbf{k}, i\omega) \cdot \tilde{\sigma}_j$ is the spin vertex function, which can be decomposed as

$$\Pi(\mathbf{k}, i\omega) \cdot \tilde{\sigma}_j \equiv \sum_m \Pi_m(\mathbf{k}, i\omega) \langle a_{jm}(E_F) \rangle \rho_m, \quad (\text{S48})$$

where $a_{im}(E_F) = \int d^2\mathbf{k} a_{im}(\mathbf{k}) \delta(\xi_{\mathbf{k}} - E_F)$ and $a_{jm}(\mathbf{k})$ is given in Sec. . A self-consistent ansatz of Π_m for the integral equation above has the form

$$\Pi_m = \lambda_m^0 + \lambda_m^1 \eta_1. \quad (\text{S49})$$

Substitute it into Eq.S47, we have

$$\lambda_m^0 = 1 + \frac{\tilde{\Delta}^2}{\tau_m(\tilde{\Delta}^2 + \tilde{\omega}^2)^{3/2}} \lambda_m^0 + \frac{i\tilde{\omega}\tilde{\Delta}}{\tau_m(\tilde{\Delta}^2 + \tilde{\omega}^2)^{3/2}} \lambda_m^1, \quad (\text{S50})$$

$$\lambda_m^1 = -\frac{i\tilde{\omega}\tilde{\Delta}}{\tau_m(\tilde{\Delta}^2 + \tilde{\omega}^2)^{3/2}} \lambda_m^0 + \frac{\tilde{\omega}^2}{\tau_m(\tilde{\Delta}^2 + \tilde{\omega}^2)^{3/2}} \lambda_m^1, \quad (\text{S51})$$

where $1/\tau_m = 1/\tau_0 - 1/\tau_{so}$ for $m = 1, 2$ and $1/\tau_m = 1/\tau_0 + 1/\tau_{so} = 1/\tau$ for $m = 3$. Then we obtain

$$\lambda_m^0 = \frac{\tilde{\omega}^2}{\tilde{\Delta}^2 + \tilde{\omega}^2} + \frac{\tilde{\Delta}^2 \tau_m}{(-\sqrt{\tilde{\Delta}^2 + \tilde{\omega}^2} + \tau_m(\tilde{\Delta}^2 + \tilde{\omega}^2))}, \quad \lambda_m^1 = \frac{-i\tilde{\omega}\tilde{\Delta}}{(\tilde{\Delta}^2 + \tilde{\omega}^2)(-1 + \tau_m\sqrt{\tilde{\Delta}^2 + \tilde{\omega}^2})}. \quad (\text{S52})$$

Simplify them with Eq.S46, we get

$$\lambda_m^0 = 1 + \frac{\Delta^2}{\Delta^2 + \omega^2} \frac{1}{\tau_m\sqrt{\Delta^2 + \omega^2} + (\tau_m/\tau - 1)}, \quad \lambda_m^1 = -\frac{i\Delta\omega}{\Delta^2 + \omega^2} \frac{1}{\tau_m\sqrt{\Delta^2 + \omega^2} + (\tau_m/\tau - 1)}. \quad (\text{S53})$$

Before proceeding to the final result, we discuss more about the vertex correction coefficients λ_m^0 and λ_m^1 here. When $\tau_{so} \rightarrow \infty$, namely, in the absence of spin-orbit scattering, we find $\lambda_m^0 = 1 + \frac{\Delta^2}{\tau_0(\Delta^2 + \omega^2)^{3/2}}$, $\lambda_m^1 = -i\frac{\Delta\omega}{\tau_0(\Delta^2 + \omega^2)^{3/2}}$. The vertex correction function in this case is $\Pi_m(i\omega) = (1 - \frac{\partial \Sigma(i\omega)}{\partial i\omega})$, which is exactly the Ward's identity. We have this identity here because without spin-orbit scattering, the vertex behaves as a scalar and spin is a conserve quantity.

After taking both the self-energy and vertex corrections, we can evaluate the disorder-averaged spin susceptibility $\overline{\chi_s^{ii}}$ from Eq.S41:

$$\overline{\chi_s^{ii}}/\chi_n^{ii} = 1 - \pi k_B T \sum_{\omega_n} \frac{\Delta^2}{(\omega_n^2 + \Delta^2)^{\frac{3}{2}}} I_{E_F}^i(\omega_n, \Delta, \tau_0, \tau_{so}), \quad (\text{S54})$$

where χ_n^{ii} is the reduced Pauli spin susceptibility and

$$I_{E_F}^i = \sum_m \frac{2 \langle a_{im}^2(E_F) \rangle}{\langle \gamma_i(E_F) \rangle} \frac{1 + \frac{1}{\tau_m\sqrt{\omega_n^2 + \Delta^2} + \tau_m/\tau - 1}}{1 + \frac{1}{\tau\sqrt{\omega_n^2 + \Delta^2}}}. \quad (\text{S55})$$

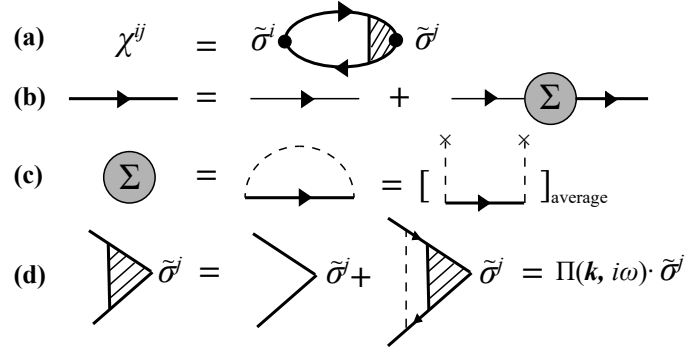


FIG. S2: Diagrammatic representation of (a) disorder-averaged spin susceptibility, (b) Dyson equation for self-energy correction, (c) self-energy in self-consistent Born approximation, (d) integral equation for spin vertex correction. The impurity potential is $U_{im}(\mathbf{k} - \mathbf{k}') = U_1(\mathbf{k} - \mathbf{k}') + U_2(\mathbf{k} - \mathbf{k}')i(\hat{\mathbf{k}} \times \hat{\mathbf{k}}') \cdot \boldsymbol{\sigma}$ [S17]. The first term describes scattering from scalar potential fluctuations, and the second term describes the spin-orbit scattering.

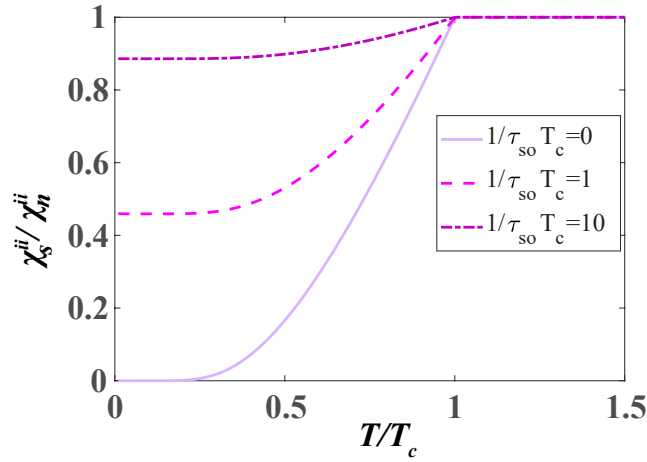


FIG. S3: Plot of χ_s^{ii}/χ_n^{ii} versus T/T_c in Eq.S57 for $i = x, y$. The strength of spin-orbit scattering is characterized by the dimensionless parameter $1/\tau_{so} T_c$. Evidently, the appearance of spin-orbit coupling generates finite residue spin susceptibility that can enhance the upper critical field.

Comparing with χ_s^{ii} in the clean case, we have an extra factor I_{EF}^i here that encodes the information of impurity scattering. When the spin-orbit scattering is absent, namely in the limit $\tau_{so} \rightarrow \infty$, we have $\tau_m = \tau_0 = \tau$, thus $I_{EF}^i = 1$ and we have

$$\overline{\chi_s^{ii}}/\chi_n^{ii} = 1 - \pi k_B T \sum_{\omega_n} \frac{\Delta^2}{(\Delta^2 + \omega_n^2)^{3/2}} = \chi_s^{ii}/\chi_n^{ii}. \quad (\text{S56})$$

Thus, without spin-orbit scattering, $\overline{\chi_s} = \chi_s$ as shown in Eq.S24 and the disorder-averaged spin susceptibility is unchanged. This can be seen directly from the ladder diagram: when the scalar Ward's identity is preserved, the self-energy correction cancels the vertex correction. This shows that the B_{c2} in SOPC superconductors is insensitive to the potential fluctuations induced by impurities.

With finite spin-orbit scattering, namely $\tau_{so}^{-1} \neq 0$,

$$I_{EF}^i(\omega_n, \Delta, \tau_0, \tau_{so}) = \frac{2 \langle a_{i3}(E_F) \rangle}{\langle \gamma_i(E_F) \rangle} + \sum_{m=1}^2 \frac{2 \langle a_{im}^2(E_F) \rangle}{\langle \gamma_i(E_F) \rangle} \frac{1 - \frac{1}{\tau_{so} \sqrt{\omega_n^2 + \Delta^2} + 2}}{1 + \frac{1}{\tau_{so} \sqrt{\omega_n^2 + \Delta^2}}}. \quad (\text{S57})$$

The coefficients $\langle a_{im}(E_F) \rangle$ and $\langle \gamma_i(E_F) \rangle$ capture the effect of SOPC on spin-orbit scattering. Plots of residue χ_s^{ii} ($i = x, y$) at different spin-orbit scattering strengths are shown in Fig.S3. Clearly, the presence of sufficiently strong spin-orbit scattering with $1/\tau_{so} \sim T_c \sim 0.1$ meV can give rise to a residue spin susceptibility to enhance the B_{c2} . However,

as the correction in χ_s does not affect the order of $\chi_n - \chi_s$, the enhancement of B_{c2} is not affected in a qualitative way given $B_{c2} = B_p \sqrt{\chi_0/(\chi_n - \chi_s)}$ as we discussed in the main text.

In conclusion, we find that B_{c2} in the SOPC superconductor is robust against scalar potential fluctuations and spin-orbit scattering may further enhance B_{c2} by inducing a residue χ_s .

POSSIBILITY OF INTER-ORBITAL PAIRINGS

In the main text, we assumed *intra-orbital* pairing which is expected to be favored when the intra-orbital attractive interaction dominates. However, given that the monolayer WTe₂ becomes superconducting near the topological band crossing points where different orbitals are strongly mixed by SOPC, instability toward *inter-orbital* pairings is also possible under inter-orbital attractive interactions and worth to be explored. In the following, we study the following properties of possible inter-orbital pairings: (i) symmetry classification, (ii) pairing instability, (iii) topological nature, and (iv) enhancement of B_{c2} . In particular, we discuss the important role of SOPC in these special properties of inter-orbital pairing.

Symmetry classification

In the Nambu basis $(c_{\mathbf{k},\uparrow}, c_{\mathbf{k},\downarrow}, c_{-\mathbf{k},\downarrow}^\dagger, -c_{-\mathbf{k},\uparrow}^\dagger)^T$ with $c_{\mathbf{k},\sigma} = (c_{p,\mathbf{k},\sigma}, c_{d,\mathbf{k},\sigma})^T$, the pairing matrix transforms as [S19, S20]

$$T : \hat{\Delta}(\mathbf{k}) \mapsto \sigma_y \hat{\Delta}^*(-\mathbf{k}) \sigma_y; \quad (\text{S58})$$

$$g : \hat{\Delta}(g\mathbf{k}) \mapsto U(g) \hat{\Delta}(\mathbf{k}) U^{-1}(g) \quad (\text{S59})$$

where $T = i\sigma_y K$ is the time-reversal operation, g is a symmetry operation in the C_{2h} point group of monolayer WTe₂. In our convention, the mirror operation σ_h defined in the usual character table of C_{2h} is the mirror reflection about the xz -plane $M_y : (x, y, z) \mapsto (x, -y, z)$. By imposing time-reversal-symmetry and fermi statistics, all possible intra-unit-cell (*i.e.*, \mathbf{k} -independent) pairing matrices are listed in Table S2 below and classified according to the irreducible representations (IRs) of C_{2h} .

TABLE S2: Classifications of all time-reversal-invariant intra-unit-cell pairings according to the irreducible representations (IRs) of C_{2h} point group for monolayer WTe₂. The pairings are written in matrix form under the Nambu basis $(c_{\mathbf{k},\uparrow}, c_{\mathbf{k},\downarrow}, c_{-\mathbf{k},\downarrow}^\dagger, -c_{-\mathbf{k},\uparrow}^\dagger)^T$ with $c_{\mathbf{k},\sigma} = (c_{p,\mathbf{k},\sigma}, c_{d,\mathbf{k},\sigma})^T$.

IRs	A_g	A_u	B_u
P	+	−	−
M_y	+	−	+
Singlet	$\eta_1 s_0, \eta_1 s_z$	None	$\eta_1 s_x$
Triplet	None	$\eta_1 s_y \sigma_x, \eta_1 s_y \sigma_z$	$\eta_1 s_y \sigma_y$

The trivial A_g phase describes the intra-orbital spin-singlet pairing we considered in the main text. The nontrivial A_u phase includes two inter-orbital triplet pairings $\hat{\Delta}_{A_u,1} = \eta_1 s_y \sigma_x$, $\hat{\Delta}_{A_u,2} = \eta_1 s_y \sigma_z$, while the other nontrivial B_u phase includes one inter-orbital spin-singlet pairing $\hat{\Delta}_{B_u,1} = \eta_1 s_x$ and one inter-orbital spin-triplet pairing $\hat{\Delta}_{B_u,2} = \eta_1 s_y \sigma_y$, respectively.

Pairing instability

To study the pairing instability under attractive interactions, we start from the general interacting Hamiltonian:

$$\hat{H}_{int} = \frac{1}{2} \sum_{\mathbf{p}, \mathbf{p}'} V_{\alpha\beta\gamma\delta}^{ijkl} \psi_{i,\alpha,-\mathbf{p}}^\dagger \psi_{j,\beta,\mathbf{p}}^\dagger \psi_{k,\gamma,\mathbf{p}'} \psi_{l,\delta,-\mathbf{p}'}. \quad (\text{S60})$$

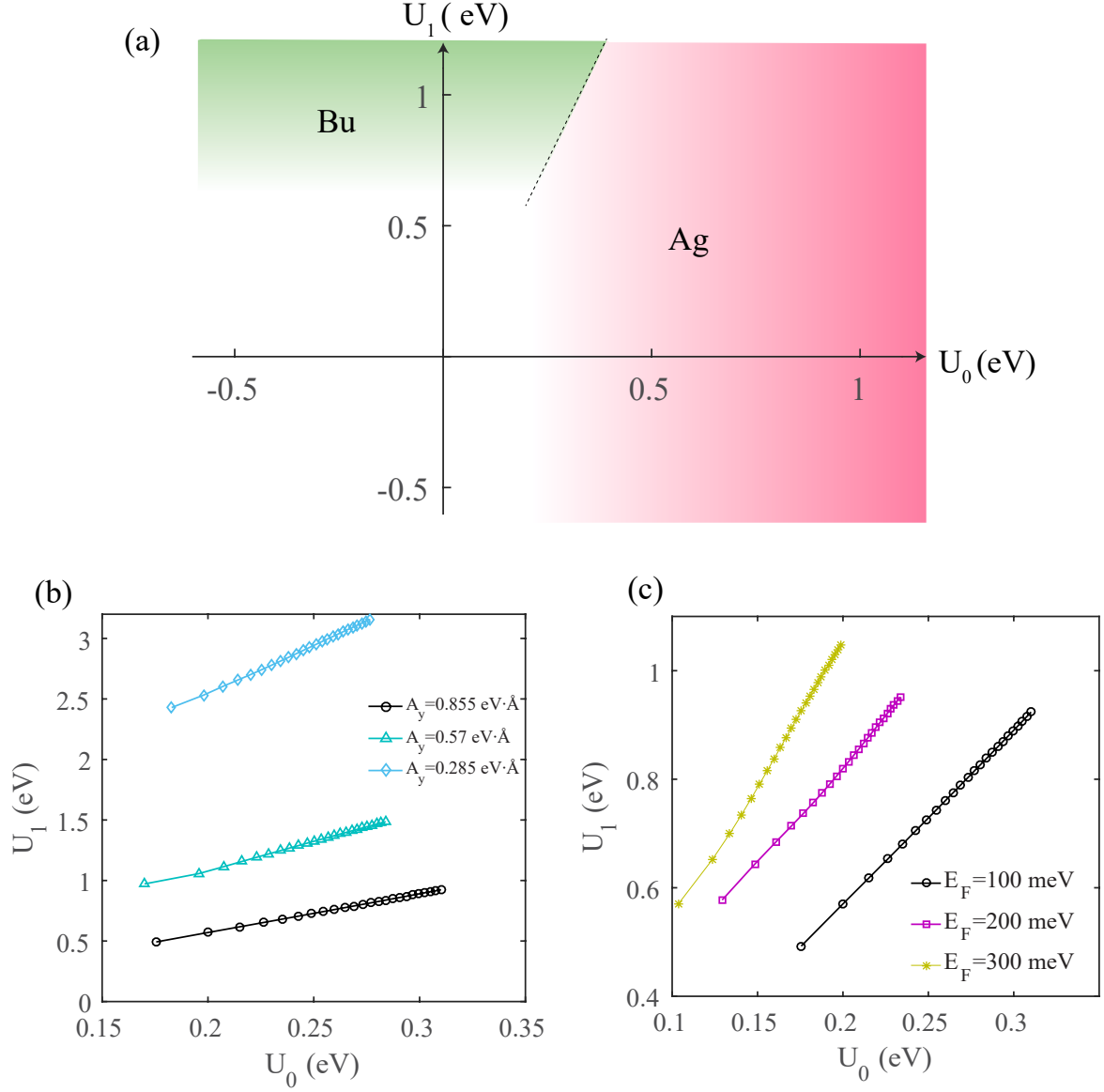


FIG. S4: (a) Superconducting phase diagram with intra-orbital $\hat{\Delta}_0$ (A_g -phase) and inter-orbital pairing $\hat{\Delta}_1$ (B_u -phase). $U_i > 0$ denotes attractive interaction ($i = 0/1$ stands for intra/inter-orbital). (b)-(c) Phase boundaries between B_u/A_g pairings under different SOPC strengths A_y and chemical potential E_F . Black dotted lines in (b)-(c) are identical to the phase boundary in (a). By reducing A_y (b) or increasing E_F (c), the SOPC effect is reduced and a larger U_1 is generally required for B_u phase to be favored.

where i, j, k, l and $\alpha, \beta, \gamma, \delta$ are the orbital and spin indices respectively. With \hat{H}_{int} respecting all point group $g \in C_{2h}$, time-reversal and SU(2) symmetries, $V_{\alpha\beta\gamma\delta}^{ijkl}$ can be decomposed into different channels as

$$V_{\alpha\beta\gamma\delta}^{ijkl} = - \sum_{\Gamma, m} V_{\Gamma, m} (\hat{\Delta}_{\Gamma, m} i\sigma_y)_{ij, \alpha\beta} (\hat{\Delta}_{\Gamma, m}^\dagger i\sigma_y)_{kl, \gamma\delta}. \quad (S61)$$

Here, Γ labels different irreducible representations (IRs), m labels the possible components in each Γ , and the forms of $\hat{\Delta}_{\Gamma, m}$ for a given (Γ, m) corresponds to one particular component in Table S2. Note that the minus sign in front of the summation captures the attractive nature of the interaction, thus $V_{\Gamma, m} > 0 (< 0)$ denotes attractive (repulsive) interaction in the given channel labelled by (Γ, m) . In each pairing phase belonging to a representation Γ , the critical

temperature is given by

$$\det \left[\begin{pmatrix} V_{\Gamma,1}\chi_{\Gamma,11}(T_c) & V_{\Gamma,1}\chi_{\Gamma,12}(T_c) \\ V_{\Gamma,2}\chi_{\Gamma,21}(T_c) & V_{\Gamma,2}\chi_{\Gamma,22}(T_c) \end{pmatrix} - I \right] = 0, \quad (\text{S62})$$

where $\chi_{\Gamma,mm'}$ denotes the pairing susceptibility:

$$\begin{aligned} \chi_{\Gamma,mm'} &= -\frac{1}{\beta} \sum_{n,\mathbf{p}} \text{Tr}(G_e(\mathbf{p}, i\omega_n) \Delta_{\Gamma,m} G_h(\mathbf{p}, i\omega_n) \Delta_{\Gamma,m'}^\dagger) \\ &= \int \frac{d^2\mathbf{p}}{(2\pi)^2} \sum_{a,b} O_{a,b}^{\Gamma m}(\mathbf{p}) O_{a,b}^{\Gamma m'}(\mathbf{p}) \frac{1 - f(E_a(\mathbf{p})) - f(E_b(-\mathbf{p}))}{E_a(\mathbf{p}) + E_b(-\mathbf{p})}. \end{aligned} \quad (\text{S63})$$

Here, the single particle electron Green's function $G_e(\mathbf{p}, i\omega_n) = (i\omega_n - H_0(\mathbf{p}))^{-1}$ and hole Green's function $G_h(\mathbf{p}, i\omega_n) = (i\omega_n + H_0(\mathbf{p}))^{-1}$, the overlap function $O_{a,b}^{\Gamma m}(\mathbf{p}) = \langle u_{a,\mathbf{p}} | \Delta_{\Gamma,m} | \nu_{b,\mathbf{p}} \rangle$ with $|u_{a,\mathbf{p}}\rangle, |\nu_{b,\mathbf{p}}\rangle$ being eigenvectors of $H_0(\mathbf{p})$ satisfying $H_0(\mathbf{p}) |u_{a,\mathbf{p}}\rangle = E_a(\mathbf{p}) |u_{a,\mathbf{p}}\rangle$, $H_0(\mathbf{p}) |\nu_{b,\mathbf{p}}\rangle = E_b(\mathbf{p}) |\nu_{b,\mathbf{p}}\rangle$, a, b are the band indices.

To further simplify our analysis, we note that the experimentally observed B_{c2} is only 1 – 3 times higher than the Pauli limit for $T \rightarrow 0$ [S22, S23], which is not compatible with triplet pairing phases: for A_u phase, the combination of two triplet pairings $\hat{\Delta}_{A_u,1} = \eta_1 s_y \sigma_x$ and $\hat{\Delta}_{A_u,2} = \eta_1 s_y \sigma_z$ are characterized by a triplet \mathbf{d} -vector of the general form $\mathbf{d} = (d_x, 0, d_z)$, which is parallel to the xz -plane and generates equal-spin Cooper pairs with spins in the y -direction [S21]. This would lead to large superconducting spin susceptibility [S13] and a divergent B_{c2} for fields along the y -direction as $T \rightarrow 0$. This motivates us to first rule out the A_u phase.

On the other hand, the B_u phase also has a triplet component $\hat{\Delta}_{B_u,2} = \eta_1 s_y \sigma_y$ with the triplet \mathbf{d} -vector: $\mathbf{d} = (0, d_y, 0)$, which generates equal-spin Cooper pairs with spins parallel to the xz -plane and leads to divergent B_{c2} for fields along the x -direction as $T \rightarrow 0$. As the singlet $\hat{\Delta}_{B_u,1} = \eta_1 s_x$ and triplet $\hat{\Delta}_{B_u,2} = \eta_1 s_y \sigma_y$ components in B_u phase can mix in general, the discrepancy between $\hat{\Delta}_{B_u,2}$ and the experimental observation further motivates us to consider the channel dominated by $\hat{\Delta}_{B_u,1} = \eta_1 s_x$. In fact, numerically we find that $\chi_{\Gamma,11} \approx \chi_{\Gamma,22}$ and the singlet-triplet mixing $\chi_{\Gamma,12} = \chi_{\Gamma,21}^*$ between $\hat{\Delta}_{B_u,1}$ and $\hat{\Delta}_{B_u,2}$ is negligibly small. Therefore, there does exist a singlet-dominant phase in B_u if $V_{B_u,1}$ dominates over $V_{B_u,2}$. We note that the condition $V_{B_u,1} \gg V_{B_u,2}$ can indeed be met under realistic considerations: by projecting the general interaction \hat{H}_{int} to the $\hat{\Delta}_{B_u,1}$ and $\hat{\Delta}_{B_u,2}$ channels, it can be shown explicitly that: $V_{B_u,1} = -(I_{pd} + J_{pd})$ and $V_{B_u,2} = -(I_{pd} - J_{pd})$, where I_{pd} and J_{pd} stand for the inter-orbital direct coupling and exchange coupling terms given by:

$$\begin{aligned} I_{pd} &= \int d\mathbf{r} d\mathbf{r}' |\phi_p(\mathbf{r})|^2 V(|\mathbf{r} - \mathbf{r}'|) |\phi_d(\mathbf{r}')|^2, \\ J_{pd} &= \int d\mathbf{r} d\mathbf{r}' \phi_p^*(\mathbf{r}) \phi_d^*(\mathbf{r}') V(|\mathbf{r} - \mathbf{r}'|) \phi_p(\mathbf{r}') \phi_d(\mathbf{r}), \end{aligned} \quad (\text{S64})$$

where $\phi_{l=p,d}(\mathbf{r})$ describes the Wannier orbital with p, d characters localized within the unit cell, and $V(|\mathbf{r} - \mathbf{r}'|) < 0$ describes the microscopic attractive interaction leading to pairing instability. To drive pairing instability toward inter-orbital pairing, the spatial overlap between Wannier p, d -orbitals is required to be strong. Thus, one expects $I_{pd} \sim J_{pd} < 0$, and $V_{B_u,1} = -(I_{pd} + J_{pd}) \gg V_{B_u,2} = -(I_{pd} - J_{pd})$, which simply reflects the fact that singlet states generally acquire a larger attractive interaction strength due to its symmetrical orbital part of the two-body wave function [S24].

Based on the observations above, we focus on the inter-orbital singlet $\hat{\Delta}_{B_u,1}$ pairing and compare its pairing instability with the intra-orbital singlet A_g phase considered in the main text. For simplicity of the following discussions, we relabel the intra-orbital interaction as $V_{A_g,1} = V_{A_g,2} = U_0$, the inter-orbital interaction as $V_{B_u,1} = U_1$, and we refer to the inter-orbital singlet $\hat{\Delta}_{B_u,1}$ pairing phase simply as the B_u phase.

The superconducting phase diagram with B_u and A_g pairing phases is shown in Fig. S4, where the more favorable phase at a given point (U_0, U_1) is determined by the phase with highest T_c . Here, $U_{i=0,1} > 0$ ($U_{i=0,1} < 0$) denotes the interaction being attractive (repulsive). The chemical potential is set to be close to the topological band crossing points as in Fig. 2 of the main text. When inter-orbital interaction is repulsive ($U_1 < 0$), an intra-orbital attraction $U_0 > 0$ leads to instability toward intra-orbital A_g phase. In contrast, when intra-orbital interaction is repulsive ($U_0 < 0$), an inter-orbital attraction $U_1 > 0$ leads to instability toward the inter-orbital B_u phase. In the regime where $U_0, U_1 > 0$, the $A_g(B_u)$ -phase is more energetically favored when $U_0(U_1)$ dominates. As the two pairing phases belong to different irreducible representations, these two pairings do not mix, and a phase transition happens at the well-defined phase boundary indicated by the dashed line in Fig. S4a.

Notably, the inter-orbital B_u -phase is sensitive to the SOPC as the effective pairing strength is controlled by the mixing between p, d -orbitals. By fixing the chemical potential near the band crossing point and reducing the SOPC strength A_y gradually, the phase boundary between B_u -phase and A_g -phase gets shifted upward (Fig. S4b). This indicates that a stronger interaction U_1 is needed for the inter-orbital B_u -pairing phase to be favored. Moreover, as we discussed in the main text, the SOPC effect is only important near the topological band crossing points. Thus, by tuning the chemical potential away from the band crossing points, the SOPC effect is reduced. In this case, the phase boundary also gets shifted upward with the regime favoring the B_u -pairing phase being reduced (Fig. S4c). These results clearly show that the SOPC helps to stabilize the B_u -phase under inter-orbital attractive interactions.

Topological nature

It is interesting to note that the B_u phase is an odd-parity pairing phase (Table S2), similar to the odd-parity pairing studied in Cu-doped Bi_2Se_3 [S19]. As we pointed out in the main text, this odd-parity pairing results in a DIII class topological superconductor when the Fermi surface encloses odd number of time-reversal-invariant (TRIM) points [S19]. Indeed, given a nonzero mean-field order parameter $\hat{\Delta}_1$ for the B_u phase, the explicit form of B_u pairing can be written as: $\hat{\Delta}_1 = \Delta_1(c_{\mathbf{k},p,\uparrow}^\dagger c_{-\mathbf{k},d,\downarrow}^\dagger - c_{\mathbf{k},p,\downarrow}^\dagger c_{-\mathbf{k},d,\uparrow}^\dagger + h.c.)$. We explicitly reveal the nontrivial topological nature of the B_u pairing below by showing that projecting $\hat{\Delta}_1$ to the MCPB basis results in an effective $p \pm ip$ pairing. For simplicity, we drop $A_z k_y$ terms in the SOPC given $A_y, A_x \gg A_z$ as shown in Table S1.

In the basis of $|\mathbf{k}, p, \uparrow\rangle, |\mathbf{k}, p, \downarrow\rangle, |\mathbf{k}, d, \uparrow\rangle, |\mathbf{k}, d, \downarrow\rangle$, the pseudospin basis is given by:

$$|\mathbf{k}, \alpha\rangle = \frac{1}{2N_{\mathbf{k}}} \begin{pmatrix} P(\mathbf{k})(e^{i\frac{\alpha\mathbf{k}}{2}} + e^{-i\frac{\alpha\mathbf{k}}{2}}) \\ e^{i\phi_{\mathbf{k}}} P(\mathbf{k})(e^{i\frac{\alpha\mathbf{k}}{2}} - e^{-i\frac{\alpha\mathbf{k}}{2}}) \\ D(\mathbf{k})e^{i\frac{\alpha\mathbf{k}}{2}} - D^*(\mathbf{k})e^{-i\frac{\alpha\mathbf{k}}{2}} \\ e^{i\phi_{\mathbf{k}}}(D(\mathbf{k})e^{i\frac{\alpha\mathbf{k}}{2}} + D^*(\mathbf{k})e^{-i\frac{\alpha\mathbf{k}}{2}}) \end{pmatrix}, \quad |\mathbf{k}, \beta\rangle = \frac{1}{2N_{\mathbf{k}}} \begin{pmatrix} e^{-i\phi_{\mathbf{k}}} P(\mathbf{k})(e^{i\frac{\alpha\mathbf{k}}{2}} - e^{-i\frac{\alpha\mathbf{k}}{2}}) \\ P(\mathbf{k})(e^{i\frac{\alpha\mathbf{k}}{2}} + e^{-i\frac{\alpha\mathbf{k}}{2}}) \\ e^{-i\phi_{\mathbf{k}}}(D(\mathbf{k})e^{i\frac{\alpha\mathbf{k}}{2}} + D^*(\mathbf{k})e^{-i\frac{\alpha\mathbf{k}}{2}}) \\ D(\mathbf{k})e^{i\frac{\alpha\mathbf{k}}{2}} - D^*(\mathbf{k})e^{-i\frac{\alpha\mathbf{k}}{2}} \end{pmatrix}, \quad (\text{S65})$$

where $e^{i\phi_{\mathbf{k}}} = (A_y k_y + iA_x k_x)/Ak$, $P(\mathbf{k}) = E(\mathbf{k}) + \mathcal{M}(\mathbf{k})$ and $D(\mathbf{k}) = ivk_x + Ak$ characterize the weights of the p and d -orbitals in the pseudospin basis. By defining $f_{p,+}(\mathbf{k}) = P(\mathbf{k})(e^{i\frac{\alpha\mathbf{k}}{2}} + e^{-i\frac{\alpha\mathbf{k}}{2}})$, $f_{p,-}(\mathbf{k}) = -iP(\mathbf{k})(e^{i\frac{\alpha\mathbf{k}}{2}} - e^{-i\frac{\alpha\mathbf{k}}{2}})$, $f_{d,+}(\mathbf{k}) = (D(\mathbf{k})e^{i\frac{\alpha\mathbf{k}}{2}} + D^*(\mathbf{k})e^{-i\frac{\alpha\mathbf{k}}{2}})$, $f_{d,-}(\mathbf{k}) = -i(D(\mathbf{k})e^{i\frac{\alpha\mathbf{k}}{2}} - D^*(\mathbf{k})e^{-i\frac{\alpha\mathbf{k}}{2}})$ [note: $f_{p,\pm}(\mathbf{k}), f_{d,\pm}(\mathbf{k})$ are all real functions of \mathbf{k} , with $f_{p,\pm}(-\mathbf{k}) = \pm f_{p,\pm}(\mathbf{k}), f_{d,\pm}(-\mathbf{k}) = \pm f_{d,\pm}(\mathbf{k})$], we project $c_{\mathbf{k},l,\sigma}^\dagger = \langle \mathbf{k}, \alpha | \mathbf{k}, l, \sigma \rangle c_{\mathbf{k},\alpha}^\dagger + \langle \mathbf{k}, \beta | \mathbf{k}, l, \sigma \rangle c_{\mathbf{k},\beta}^\dagger$ with $l = p, d, \sigma = \uparrow, \downarrow$, and $\hat{\Delta}_1$ is reduced to:

$$\hat{\Delta}_{1,eff}(\mathbf{k}) = \Delta_1 \frac{f_{p,-}(\mathbf{k})f_{d,-}(\mathbf{k}) + f_{p,+}(\mathbf{k})f_{d,+}(\mathbf{k})}{4N_{\mathbf{k}}^2 Ak} \left[(A_y k_y - iA_x k_x) c_{\mathbf{k},\alpha}^\dagger c_{-\mathbf{k},\alpha}^\dagger - (A_y k_y + iA_x k_x) c_{\mathbf{k},\beta}^\dagger c_{-\mathbf{k},\beta}^\dagger \right]. \quad (\text{S66})$$

Clearly, $\hat{\Delta}_{1,eff}(\mathbf{k})$ reveals that the combined effect of $\hat{\Delta}_1$ and SOPC leads to an effective $p \pm ip$ pairing. Notably, in the absence of SOPC ($A_y = A_x = 0$) or $\hat{\Delta}_1$ ($\Delta_1 = 0$), the effective p -wave gap function $\hat{\Delta}_{1,eff}(\mathbf{k})$ vanishes and the bulk spectrum of Bogoliubov quasi-particles remains gapless. Thus, when the Fermi surface encloses odd number of TRIM-points, the effective $p \pm ip$ pairing leads to a time-reversal-invariant topological superconductor.

Unfortunately, as we pointed out in the main text, superconductivity in monolayer WTe_2 sets in when the conduction bands near Q-points are filled (Fig. S5a), where the Fermi surface consists of two disconnected Fermi pockets enclosing none of the four TRIM points Γ, X, Y, Z (Fig. S5b). As a result, the system remains topologically trivial. To demonstrate this explicitly, we use a tight-binding model to calculate the energy spectrum of a finite WTe_2 strip under $\hat{\Delta}_1$. Clearly, no helical Majorana modes can form on the edge as shown in Fig. S5c. To reveal the nontrivial nature of $\hat{\Delta}_1$, we artificially tune the chemical potential to the hole bands (Fig. S5d) such that the Γ -point is enclosed by the Fermi surface (Fig. S5e). In this case, helical Majorana states emerge on the edge (Fig. S5f), which clearly shows that the system becomes a DIII class topological superconductor. Details of the tight-binding model used to obtain the edge state spectrum in Fig. S5 are presented in subsection E of this Supplementary Material.

As an explanatory note, we point out that the mechanism behind the generation of effective p -wave pairing from a singlet-pairing $\hat{\Delta}_1$ in the orbital-basis is similar to the effective p -wave pairing created by s -wave pairing and strong noncentrosymmetric spin-orbit couplings (SOCs) [S13, S21, S25]. From the symmetry point of view, such phenomena arises from the breaking of both inversion and $SU(2)$ spin-rotation symmetries. In the case of noncentrosymmetric superconductors, the noncentrosymmetric SOC in the normal state breaks both inversion and $SU(2)$, while in the case of the B_u phase in superconducting WTe_2 , the inversion-breaking due to $\hat{\Delta}_1$ and $SU(2)$ -breaking from SOPC work together to produce the effective p -wave pairing.

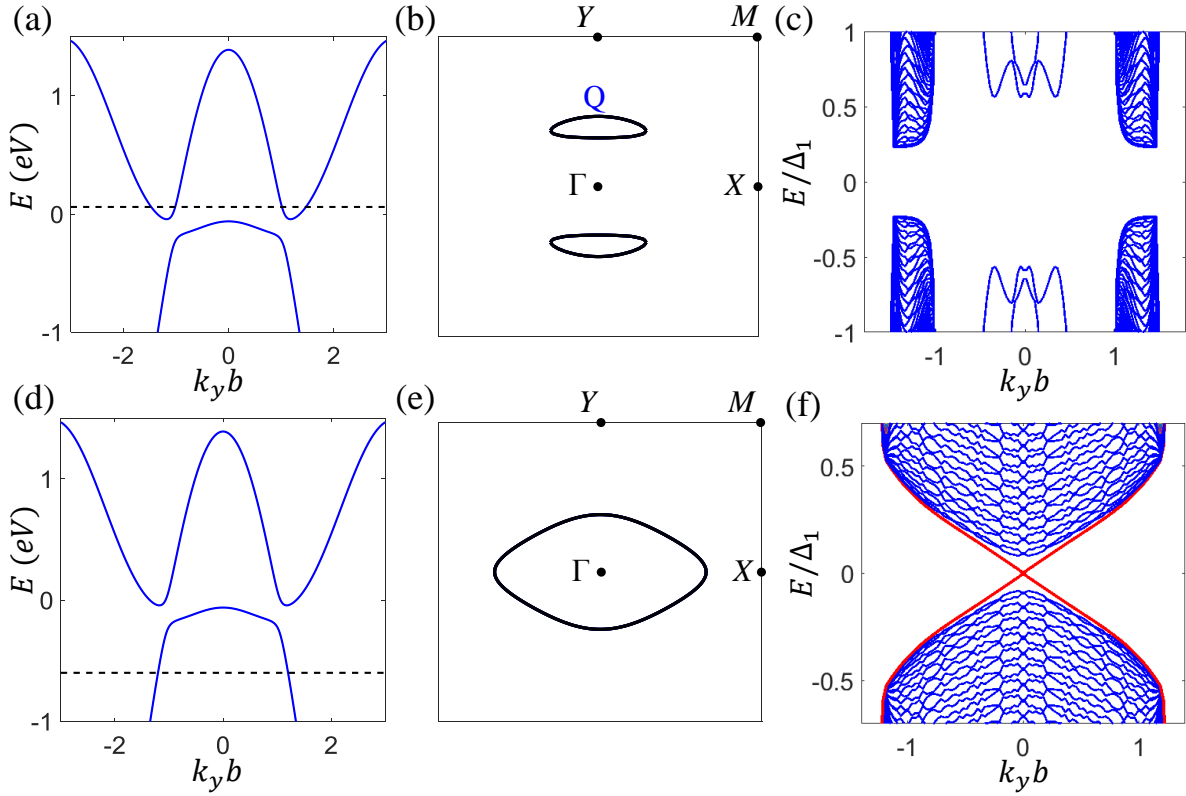


FIG. S5: Spectrum of a strip of superconducting WTe₂ in B_u pairing phase with pairing amplitude Δ_1 . (a) Under realistic conditions, WTe₂ becomes superconducting when conduction band states near the Q-points are filled, where the Fermi surface is formed by two disconnected Q-pockets enclosing none of the TRIM-points (b). In this case, no helical Majorana modes can form on the edge (c). By artificially tuning the chemical potential to the hole band (d) such that the Γ -point is enclosed by the Fermi surface (e), the system becomes a DIII class topological superconductor with helical Majorana modes on the edge (f). Details of the tight-binding model used in (a)-(f) are presented in subsection E of this Supplementary Material.

Moreover, the odd-parity nature of $\hat{\Delta}_1$ forbids any pseudospin-singlet pairing in the effective pairing Hamiltonian: given a general effective pairing $\hat{\Delta}_{eff}(\mathbf{k}) = \psi(\mathbf{k})\rho_0 + \mathbf{d}(\mathbf{k}) \cdot \boldsymbol{\rho}$ under pseudospin basis, parity transforms $\hat{\Delta}_{eff}(\mathbf{k})$ as: $\hat{\Delta}_{eff}(\mathbf{k}) \mapsto \hat{\Delta}_{eff}(-\mathbf{k})$, while fermi statistics requires $\psi(\mathbf{k}) = \psi(-\mathbf{k})$, $\mathbf{d}(\mathbf{k}) = -\mathbf{d}(-\mathbf{k})$. As the odd-parity condition imposes $\hat{\Delta}_{eff}(\mathbf{k}) = -\hat{\Delta}_{eff}(-\mathbf{k})$, the pseudospin singlet component is forced to vanish: $\psi(\mathbf{k}) = 0$. As we discuss next, the pseudospin triplet component in $\hat{\Delta}_{1,eff}(\mathbf{k})$ under the odd-parity B_u phase has important consequences on the spin magnetic properties of superconducting WTe₂.

Enhancement of B_{c2}

Finally, we show how $\hat{\Delta}_1$ under B_u pairing phase affects the in-plane B_{c2} . As we discussed in the main text, when states near Q-points are filled, there is a large anisotropy in the SOPC: $A_y k_y \gg A_x k_x, A_z k_z \sim 0$. In other words, the k_y -component in the effective $p \pm ip$ pairing dominates near Q-points (Eq.S66). This allows us to approximately set $\theta_{\mathbf{k}} = \pi/2$, $\sin \phi_{\mathbf{k}} = 0$ and the components in the \mathbf{d} -vector under pseudospin basis are given by:

$$d_x(\mathbf{k}) = -\Delta_1(E(\mathbf{k}) + \mathcal{M}(\mathbf{k}))A_y k_y / N_{\mathbf{k}}^2, \quad d_y(\mathbf{k}) = d_z(\mathbf{k}) = 0. \quad (\text{S67})$$

Notably, the spin magnetic property of the superconducting state is determined by the spin structure of pairing electrons in the real spin basis. To see how $\hat{\Delta}_1$ affects the spin properties of Cooper pairs formed by electrons near the Fermi surface, we need to study how the real-spin triplet $\tilde{\mathbf{d}}$ -vector is related to the pseudospin triplet \mathbf{d} -vector in Eq.S67. Recall that any component $\tilde{d}_i (i = x, y, z)$ of a real-spin triplet $\tilde{\mathbf{d}}$ -vector is given by: $\tilde{d}_i(\mathbf{k}) = \text{Tr}[\sigma_i \hat{\Delta}_t(\mathbf{k})]/2$, where $\hat{\Delta}_t(\mathbf{k}) = \tilde{\mathbf{d}}(\mathbf{k}) \cdot \boldsymbol{\sigma}$ is the usual real-spin triplet pairing characterized by a nonzero $\tilde{\mathbf{d}}$ and σ_i are the Pauli matrices

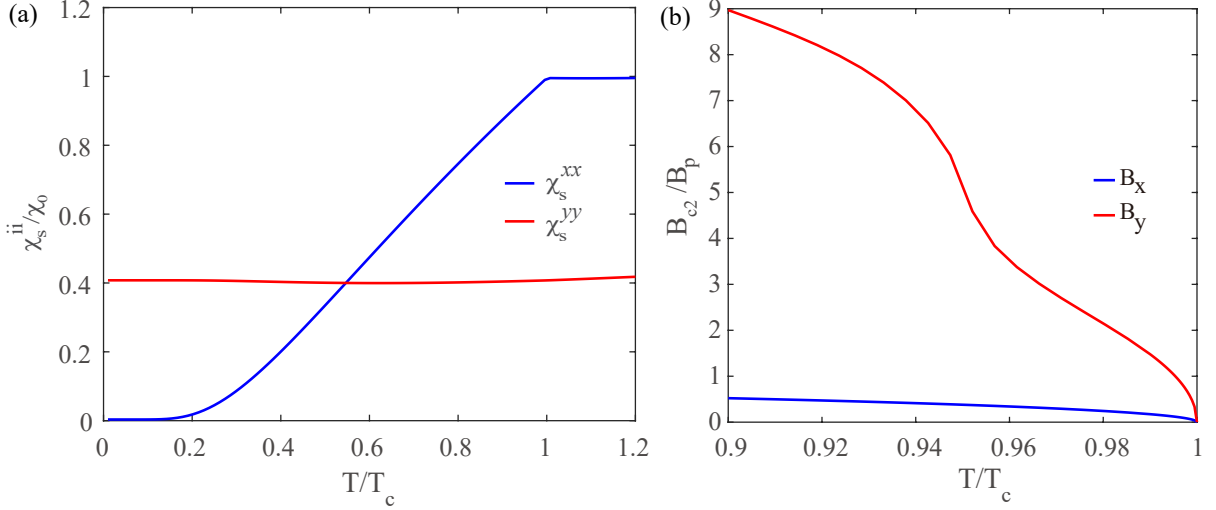


FIG. S6: Spin susceptibility and upper critical field for the B_u pairing. (a) Superconducting spin susceptibility χ_s^{ii} ($i = x, y$) as a function of temperature T . (b) The upper critical field B along x, y - direction as a function of temperature T obtained from solving linearized gap equations numerically. Except for the pairing form, other parameters are the same with the Fig. 3a of main text.

for real spins. Therefore, in the pseudospin basis representation, the components of real-spin $\tilde{\mathbf{d}}$ is given by

$$\tilde{d}_i(\mathbf{k}) = \frac{1}{2} \text{Tr}[\tilde{\sigma}_i(\mathbf{k}) \hat{\Delta}_{1,eff}(\mathbf{k})] \approx a_{ix}(\mathbf{k}) d_x(\mathbf{k}), \quad (\text{S68})$$

where $\tilde{\sigma}_i(\mathbf{k})$ are the real-spin Pauli matrices under pseudospin basis presented in Eq.S13, and $a_{ix}(\mathbf{k})$ are the coefficients associated with σ_i and ρ_x . Notably, with the approximation $\theta_{\mathbf{k}} = \pi/2, \sin \phi_{\mathbf{k}} = 0$, we have $\tilde{\sigma}_x = \rho_x, \tilde{\sigma}_y(\mathbf{k}) = |W_{\mathbf{k}}| \rho_y, \tilde{\sigma}_z(\mathbf{k}) = |W_{\mathbf{k}}| \rho_z$, where $W_{\mathbf{k}}$ is defined in Eq.S13. As such, we have $a_{xx} = 1, a_{yx} = a_{zx} = 0$, and the real-spin triplet $\tilde{\mathbf{d}}$ -vector in this particular case is indeed almost identical to the pseudospin triplet \mathbf{d} -vector: $\tilde{\mathbf{d}} \approx \mathbf{d} = (d_x(\mathbf{k}), 0, 0)$ which has a nonzero $\tilde{d}_x(\mathbf{k})$ -component. This nonzero $\tilde{d}_x(\mathbf{k})$ generates equal-spin Cooper pairs with spins parallel to the yz -plane, similar to the case of Ising superconductors where the nonzero $d_z(\mathbf{k})$ due to Ising SOC generates equal-spin Cooper pairs with spins parallel to the xy -plane [S21]. Therefore, under $\hat{\Delta}_1$ pairing there exists a large χ_s^{yy} in the superconducting state and the in-plane B_{c2} along y -direction is expected to be enhanced much more dramatically and diverge in the $T \rightarrow 0$ limit.

To verify our analysis above based on the pseudospin basis, we explicitly demonstrate the effect of $\hat{\Delta}_1$ on the spin magnetic properties and B_{c2} of the superconducting WTe₂. To be specific, based on the full $H_{BdG}(\mathbf{k})$ in Eq.S2 with the pairing matrix replaced by $\hat{\Delta}_1 = \Delta_1 \eta_1 s_x$, we calculate the superconducting spin susceptibility numerically using the Kubo formula

$$\chi_s^{ii} = -\frac{1}{2} u_B^2 \lim_{\mathbf{q} \rightarrow 0} \sum_{\mathbf{k}, m=n} \sum_{a,b} \frac{f(E_m(\mathbf{k})) - f(E_n(\mathbf{k} + \mathbf{q}))}{E_m(\mathbf{k}) - E_n(\mathbf{k} + \mathbf{q})} \langle n, \mathbf{k}, b | \sigma^i | m, \mathbf{k}, a \rangle \langle m, \mathbf{k}, a | \sigma^i | n, \mathbf{k}, b \rangle, \quad (\text{S69})$$

where $f(E)$ is the Fermi distribution function, eigenenergies $E_n(\mathbf{k})$ and eigenstates $|n, \mathbf{k}, a\rangle$ are calculated from the full four-band BdG Hamiltonian $H_{BdG}(\mathbf{k})$ at zero field, $a = 1, 2$ labels the two degenerate states. The superconducting spin susceptibility χ_s^{xx} and χ_s^{yy} under $\hat{\Delta}_1$ pairing as a function of temperature T are shown in Fig. S6. Notably, the superconducting spin susceptibility χ_s^{xx} along the x -direction under $\hat{\Delta}_1$ is similar to the case with intra-orbital A_g pairing in Fig.3 of the main text (blue line in Fig. S6a). This is because $\tilde{d}_x(\mathbf{k})$ generates no equal-spin Cooper pairs with spins pointing to the x -direction. Consistently, B_{c2} under B_x is also similar to the case with intra-orbital pairing (blue line in Fig. S6b). In sharp contrast, χ_s^{yy} along the y -direction is non-vanishing in the $T \rightarrow 0$ limit, and remains nearly the same as its normal state value χ_n^{yy} (red line in Fig. S6a), indicating the superconductivity is insensitive to the in-plane field along the y -direction. Consequently, B_{c2} under B_y gets dramatically enhanced in the $\hat{\Delta}_1$ phase belonging to the B_u representation, which easily exceeds the Pauli limit by nearly ten times even in the high temperature regime $T = 0.9T_c$ (red line in Fig. S6b). As such a dramatic enhancement in B_{c2} was not observed in the experiment, we believe the intra-orbital A_g pairing we assumed in the main text provides a more plausible description of the superconducting state in monolayer WTe₂.

We further note that with the A_g intra-orbital singlet pairing discussed in the main text, the effective BdG model under the pseudospin basis describes an s -wave superconductor with even-parity pairing, which is known to be topologically trivial and thus distinct from the odd-parity pairing studied in Cu-doped Bi_2Se_3 [S19]. In this trivial A_g phase, the quantum spin Hall edge states will acquire a full pairing gap and no helical Majorana edge modes can form. However, by placing a ferromagnetic insulator to cover half of the superconducting quantum spin Hall insulator, a Majorana fermion can form at the ferromagnet-superconductor interface [S26].

As we explained in the subsections above, the odd-parity B_u pairing has a similar topological nature as the odd-parity pairing studied in Cu-doped Bi_2Se_3 . However, the edge states will still be gapped out when the disconnected Q -valleys are filled and no TRIM point is enclosed by the Fermi surface, as shown explicitly in Fig.S5c. When the Fermi surface encloses an odd number of TRIM points, the chemical potential is generally lying deep in the bulk bands. In this case, the quantum spin Hall edge states have already merged deeply into the bulk and do not participate in the edge physics. However, since the superconducting phase is topological, helical Majorana mode will emerge in this DIII class topological superconductor as shown in Fig.S5f.

Four-band tight-binding model for superconducting WTe_2

In this subsection, we present details of the tight-binding model used to study the bulk-edge correspondence in the nontrivial B_u phase in Fig.S5. In the Nambu basis $(c_{\mathbf{k},p,\uparrow}, c_{\mathbf{k},p,\downarrow}, c_{\mathbf{k},d,\uparrow}, c_{\mathbf{k},d,\downarrow}, c_{-\mathbf{k},p,\uparrow}^\dagger, c_{-\mathbf{k},p,\downarrow}^\dagger, c_{-\mathbf{k},d,\uparrow}^\dagger, c_{-\mathbf{k},d,\downarrow}^\dagger)^T$, where $c_{\mathbf{k},l,\sigma}^\dagger$ ($l = p, d, \sigma = \uparrow, \downarrow$) creates a Bloch state formed by linear combinations of Wannier orbital of character l and spin σ , the momentum-space tight-binding Hamiltonian $\hat{H}_{BdG}^{TB}(\mathbf{k})$ for superconducting monolayer WTe_2 under $\hat{\Delta}_1$ reads:

$$\hat{H}_{BdG}^{TB}(\mathbf{k}) = \sum_{\mathbf{k},mn} c_{\mathbf{k},m}^\dagger H_{0,mn}^{TB}(\mathbf{k}) c_{\mathbf{k},n} + \Delta_1 (c_{\mathbf{k},p,\uparrow}^\dagger c_{-\mathbf{k},d,\downarrow}^\dagger - c_{\mathbf{k},p,\downarrow}^\dagger c_{-\mathbf{k},d,\uparrow}^\dagger + h.c.). \quad (\text{S70})$$

Here, $m, n = (l, \sigma)$ label the index for different Wannier orbitals with $l = p, d, \sigma = \uparrow, \downarrow$. $H_0^{TB}(\mathbf{k})$ is a 4×4 matrix given by:

$$H_0^{TB}(\mathbf{k}) = \begin{pmatrix} E_p(\mathbf{k}) - \mu & 0 & -iv_0 \sin(k_x a) + \alpha_z \sin(k_y b) & -i\alpha_x \sin(k_x a) + \alpha_y \sin(k_y b) \\ & E_p(\mathbf{k}) - \mu & i\alpha_x \sin(k_x a) + \alpha_y \sin(k_y b) & -iv_0 \sin(k_x a) - \alpha_z \sin(k_y b) \\ & & E_d(\mathbf{k}) - \mu & 0 \\ h.c. & & & E_d(\mathbf{k}) - \mu \end{pmatrix}, \quad (\text{S71})$$

where

$$\begin{aligned} E_p(\mathbf{k}) &= 2t_{1p} \cos(k_x a) + 2t_{2p} \cos(k_y b) - u_p - 2(t_{1p} + t_{2p}), \\ E_d(\mathbf{k}) &= 2t_{1d} \cos(k_x a) + 2t_{2d} \cos(k_y b) + 2t'_{2d} \cos(2k_y b) - u_d - 2(t_{1d} + t_{2d} + t'_{2d}). \end{aligned} \quad (\text{S72})$$

The parameters in $H_0^{TB}(\mathbf{k})$ above are tabulated in Table S3 below. It can be verified in a straightforward way that $H_0^{TB}(\mathbf{k})$ reduces to the $\mathbf{k} \cdot \mathbf{p}$ model near the Γ -point in Eq.S1 in the continuum limit $a, b \rightarrow 0$.

To obtain the edge spectrum in Fig.S5, we perform partial Fourier transform: $c_{k_y, m}(x) = (1/\sqrt{L_x}) \sum_{k_x} e^{-ik_x x} c_{\mathbf{k}, m}$ and set open boundary conditions for edges terminated at $x = 0$ and $x = L_x = 400$. In Fig.S5a-c, we set $\mu = 60$ meV such that two Q -pockets form at the Fermi surface. In Fig.S5d-f, we set $\mu = -0.6$ eV such that the hole band is accessed with a single Γ -pocket, and the pairing amplitude for $\hat{\Delta}_1$ in Fig.S5f is set to be $\Delta_1 = |\mu|/10$.

TABLE S3: Tight-binding parameters in $H_0^{TB}(\mathbf{k})$ (Eq.S71) in units of eV. Lattice constants: $a = 6.31\text{\AA}$, $b = 3.49\text{\AA}$.

u_p	u_d	t_{1p}	t_{2p}	t_{1d}	t_{2d}	t'_{2d}	v_0	α_x	α_y	α_z
-1.39	0.062	0.626	1.517	-0.06	-0.387	0.15	0.371	0.027	0.163	0.020

* These authors contributed equally to this work.

† Corresponding author.

phlaw@ust.hk

- [S1] X. Qian, J. Liu, L. Fu, and J. Li, *Science* **346**, 1314 (2014).
- [S2] S. Tang et al., *Nature Physics* **13**, 683 (2017).
- [S3] L. Muechler, A. Alexandradinata, T. Neupert, and R. Car, *Phys. Rev. X* **6**, 041069 (2016).
- [S4] X. Lin and J. Ni, *Phys. Rev. B* **95**, 245436 (2017).
- [S5] D.-H. Choe, H.-J. Sung, and K. J. Chang, *Phys. Rev. B* **93**, 125109 (2016).
- [S6] L.-k. Shi and J. C. W. Song, *Phys. Rev. B* **99**, 035403 (2019).
- [S7] In the usual convention, the p/d -orbital has odd/even spatial parity and the inversion operator has the form $P_z = -s_z$. As the extra sign amounts to a $U(1)$ phase which can always be gauged away, we drop the minus sign throughout this Supplementary Material for convenience.
- [S8] C.-X. Liu, X.-L. Qi, H. Zhang, X. Dai, Z. Fang, and S.-C. Zhang, *Phys. Rev. B* **82**, 045122 (2010).
- [S9] J. W. F. Venderbos, V. Kozii, and L. Fu, *Phys. Rev. B* **94**, 180504 (2016).
- [S10] L. Fu, *Phys. Rev. Lett.* **115**, 026401 (2015).
- [S11] S.-K. Yip, *Phys. Rev. B* **87**, 104505 (2013).
- [S12] S.-K. Yip, arXiv:1609.04152 (2016).
- [S13] P. A. Frigeri, D. F. Agterberg and M. Sigrist, *New Journal of Physics* **6**, 115 (2004).
- [S14] A. Abrikosov and L. Gor'kov, *Sov. Phys. JETP* **15**, 752 (1962).
- [S15] R. A. Klemm, A. Luther, and M. R. Beasley, *Phys. Rev. B* **12**, 877 (1975).
- [S16] B. Dóra, A. Virosztek, and K. Maki, *Phys. Rev. B* **66**, 115112 (2002).
- [S17] A. V. Balatsky, I. Vekhter, and J.-X. Zhu, *Rev. Mod. Phys.* **78**, 373 (2006).
- [S18] A. Abrikosov and L. Gorkov, *Sov. Phys. JETP* **8**, 1090 (1959).
- [S19] L. Fu and E. Berg, *Phys. Rev. Lett.* **105**, 097001 (2010).
- [S20] J. W. F. Venderbos, V. Kozii, and L. Fu, *Phys. Rev. B* **94**, 180504(R) (2016).
- [S21] B. T. Zhou, N. F. Q. Yuan, H.-L. Jiang, and K. T. Law, *Phys. Rev. B* **93**, 180501 (2016).
- [S22] V. Fatemi, S. Wu, Y. Cao, L. Bretheau, Q. D. Gibson, K. Watanabe, T. Taniguchi, R. J. Cava and P. Jarillo-Herrero, *Science* **362**, 926-929 (2018).
- [S23] E. Sajadi, T. Palomaki, Z. Fei, W. Zhao, P. Bement, C. Olsen, S. Luescher, X. Xu, J. A. Folk and D. H. Cobden, *Science* **362**, 922-925 (2018).
- [S24] Tinkham, Michael. *Superconductivity* by M. Tinkham. New York: Gordon and Breach (1965).
- [S25] Jason Alicea, *Phys. Rev. B* **81**, 125318 (2010).
- [S26] Liang Fu and C. L. Kane, *Phys. Rev. B* **79**, 161408 (2009).